



Mathematical Modeling of Diffusion of a Hydrophilic Ionic Fertilizer in Plant Cuticles: Surfactant and Hygroscopic Effects

E. C. Tredenick^{1*}, T. W. Farrell^{1,2*} and W. A. Forster³

¹ School of Mathematical Sciences, Queensland University of Technology, Brisbane, QLD, Australia, ² ARC Centre of Excellence for Mathematical and Statistical Frontiers, Queensland University of Technology, Brisbane, QLD, Australia, ³ Plant Protection Chemistry NZ Ltd., Rotorua, New Zealand

OPEN ACCESS

Edited by:

Sanna Sevanto,
Los Alamos National Laboratory
(DOE), United States

Reviewed by:

John A. Morgan,
Purdue University, United States
Mauricio Hunsche,
Universität Bonn, Germany
Antonio Heredia,
Universidad de Málaga, Spain

*Correspondence:

E. C. Tredenick
eloise.tredenick@qut.edu.au
T. W. Farrell
t.farrell@qut.edu.au

Specialty section:

This article was submitted to
Plant Biophysics and Modeling,
a section of the journal
Frontiers in Plant Science

Received: 04 May 2018

Accepted: 06 December 2018

Published: 20 December 2018

Citation:

Tredenick EC, Farrell TW and
Forster WA (2018) Mathematical
Modeling of Diffusion of a Hydrophilic
Ionic Fertilizer in Plant Cuticles:
Surfactant and Hygroscopic Effects.
Front. Plant Sci. 9:1888.
doi: 10.3389/fpls.2018.01888

The agricultural industry requires improved efficacy of sprays being applied to crops and weeds to reduce their environmental impact and increase financial returns. One way to improve efficacy is by enhancing foliar penetration. The plant leaf cuticle is the most significant barrier to agrochemical diffusion within the leaf. The importance of a mechanistic mathematical model has been noted previously in the literature, as each penetration experiment is dictated by its specific parameters, namely plant species, environmental conditions such as relative humidity and spray formulation including adjuvant addition. A mechanistic mathematical model has been previously developed by the authors, focusing on plant cuticle diffusion of calcium chloride through tomato fruit cuticles including pore swelling, ion binding and evaporation, along with the ability to vary the active ingredient concentration and type, relative humidity and plant species. Here we further develop this model to include adjuvant effects as well as the hygroscopic nature of deliquescent ionic solutions with evaporation on the cuticle surface. These modifications to a penetration and evaporation model provide a novel addition to the literature and allow the model to be applied to many types of evaporating ionic hygroscopic solutions on many types of substrates, not just plant cuticles. We validate our theoretical model results against appropriate experimental data, discuss key sensitivities and relate theoretical predictions to physical mechanisms. The important governing mechanisms influencing surfactant enhanced penetration of ionic active through plant cuticles were found to be aqueous pore radius, pore density, cuticle thickness and initial contact angle of the applied droplet; ion binding, relative humidity and evaporation including hygroscopic water absorption parameters for point of deliquescence. The sensitivity analysis indicated surfactants increase penetration by changing the point of deliquescence of a solution, which alters the water absorption and the initial contact angle, which alters the number of pores under the droplet. The results of the validation and sensitivity analysis imply that this model accounts for many of the mechanisms governing penetration in plant cuticles.

Keywords: plant cuticle, ionic active ingredient, porous diffusion, adsorption, mathematical model, aqueous pores, penetration, surfactant

1. INTRODUCTION

The agricultural industry requires improved efficacy of sprays applied to crops and weeds (Shaner and Beckie, 2014). Application by spraying is known to be effective yet often inefficient (Knoche, 1994). Improving spray efficacy can provide significant gains, including maximized crop yield and reduced: amount of active ingredient (AI) needed, spray run-off, spray volume, residues and cost (Balneaves et al., 1993; Schönherr, 2006; McKenna et al., 2013).

The plant cuticle is a dynamic structure present on the exterior of aerial plants and is considered the rate-limiting barrier to agrochemical diffusion through plant leaves (Schönherr and Riederer, 1989). It forms a protective barrier that is modified by the environment and regulates water loss (Riederer and Schreiber, 2001; Kerstiens, 2010; Yeats et al., 2012). The plant cuticle is a lamellate, porous, highly heterogeneous structure that changes in thickness, chemical composition, adaxial and abaxial cuticle surfaces, abundance and arrangement of structures such as aqueous pores between various plant species (Buchholz, 2006; Schreiber et al., 2006; Jeffree, 2008; Kerstiens, 2010). Plant species variations have a profound effect on cuticle surface structures such as trichomes, stomata, waxes and folds that affect the wettability (Koch et al., 2008) and consequently the initial contact angles of spray droplets applied to these surfaces (Nairn et al., 2013). Cuticle thickness varies significantly between species (Jeffree, 2008) and affects penetration (Schreiber and Schönherr, 2009, p. 31) of hydrophilic ionic AIs (Santier and Chamel, 1992).

Aqueous pores are dynamic structures within the cuticle that form only in the presence of water (Riederer and Schreiber, 2001; Schönherr, 2006). They are crucial for foliar penetration of agrochemicals (Schönherr, 2006). The maximum pore size changes between plant species, with estimates between 0.3 nm in *Hedera helix L.* (Popp et al., 2005) and 2.12 nm in tomato fruit cuticle membranes (Beyer et al., 2005; Schreiber and Schönherr, 2009, p. 87). These pores are classified as nanopores (Mays, 2007; Loucks et al., 2012).

Here we will focus on agrochemicals including plant hormones, growth regulators, plant nutrients [for example calcium chloride (CaCl_2)] and pesticides such as bentazon and glyphosate that are ionic hydrophilic compounds (ionic AIs). These ionic AIs include adjuvants in the spray formulation and penetrate exclusively through aqueous pores (Schönherr and Schreiber, 2004; Schönherr, 2006) in isolated astomatous plant cuticles. Ionic AI penetration has been said to have major practical importance to the agricultural industry and significantly less is known about penetration of ionic AIs through the plant cuticle (Schreiber, 2005) but enough governing mechanisms have been defined to conduct theoretical modeling.

Ionic AIs travel through the plant cuticle via Fickian diffusion in aqueous pores (Baur, 1999; Schönherr, 2006; Schreiber and Schönherr, 2009). The concentration gradient is the driving force of diffusion (Riederer and Muller, 2008). Applying this to AI penetration in plant cuticles, an unequal distribution of ions across the cuticle creates a concentration gradient, which causes solutes to move along this concentration gradient. Water crosses

the cuticle in aqueous pores via diffusion (Schreiber et al., 2006) and is also adsorbed to the aqueous pore walls as a monolayer (Luque et al., 1995; Kerstiens, 2006).

Ion binding to the cuticle surface can significantly alter penetration. When ions are bound to the cuticle surface, they are trapped and cannot travel through the cuticle. When calcium ion penetration was measured through isolated astomatous tomato fruit cuticles (*Lycopersicon esculentum*), application onto the outside surface of the cuticle produced about 3.5 times more penetration than the inside surface after 40 h (Yamada et al., 1964). A 10% difference between the penetration of glyphosate applied to the outer (highest) and inner surfaces of tomato fruit (*Lycopersicon esculentum Mill.*) cuticles at a relative humidity close to saturation after 4 days was found (Santier and Chamel, 1992). Another preliminary study found a 60% difference between the penetration of phosphorus acid (phosphite) applied onto the abaxial (highest) and adaxial whole kauri plant leaves (both were applied to the outer surfaces) (Horgan, 2017).

Adjuvants are the broad category of chemicals added to spray tank formulations to change the AIs efficacy or spray characteristics (Hazen, 2000). Adjuvants can be wetting agents, surfactants, humectants or a combination. It is important to consider the effect of adjuvant addition with ionic AI penetration. Most experiments that include some sort of adjuvant find penetration of AI is significantly increased (Schönherr, 2001; Schönherr and Lubber, 2001).

Surfactants are forms of adjuvants that modify liquids surface characteristics (Hazen, 2000). They change the contact area, contact angle and surface tension of applied droplets (Gaskin et al., 2005). They improve emulsifying by keeping solutions well mixed and improve dispersing, spreading and wetting (Hazen, 2000). Surfactants are known to decrease an AI's point of deliquescence (POD), allowing further penetration to occur at lower relative humidity. Adding surfactants to a NaCl solution decreased the POD from 75%RH to 71%RH (Chen and Lee, 2001). Surfactants including vegetable oils such as ethoxylated rapeseed oil (RSO) are known to delay evaporation, alter the droplet surface tension and initial contact angle (Hazen, 2000; Haefs et al., 2002), produce a more homogeneous droplet footprint, increase the initial droplet area and subsequent droplet residue area, maintain sufficient relative humidity at the AI/cuticle interface and allow a paste-like deposit that is sufficiently wet to promote penetration over longer periods (Kraemer et al., 2009).

Relative humidity can significantly alter penetration of ionic AIs through plant cuticles. This is thought to be due to hydration of the cuticle, due to water adsorption to the aqueous pore walls (Luque et al., 1995; Kerstiens, 2006; Schönherr, 2006). High relative humidity is thought to promote pore swelling and increase the number and radius of aqueous pores, which generally leads to increased penetration (Middleton and Sanderson, 1965; Schönherr and Schmidt, 1979; Schönherr, 2000, 2002, 2006; Ramsey et al., 2005). Relative humidity also impacts the rate of spray droplet evaporation and hygroscopic water absorption (Tang et al., 1997).

Ionic compounds can absorb water in both liquid and vapor form from the air, due to their strong attractive forces for

the highly polar water molecules. Calcium chloride's moisture absorption is 14 times its weight in water at 95%RH. A quantitative measure of the ability to absorb water molecules from the air, termed hygroscopicity, is given by the POD of an ionic substance. If the relative humidity is above the POD of a salt, solid crystals will absorb moisture from the air until they dissolve and remain in solution (Tang et al., 1997; Oxy Chemical Company, 2014; Absortech, 2015). The solution will continue to absorb water from the air until an equilibrium is reached between the vapor pressure of the solution and the air. Crystals of CaCl_2 have been found to increasingly absorb water over several hours (Bouzenada et al., 2016). If the relative humidity then increases, more water will be absorbed by the solution. However, if the relative humidity then decreases, water will evaporate from the solution to the air and crystals will start to form when the relative humidity goes below the POD (Tang et al., 1997; Oxy Chemical Company, 2014). For example, the POD of CaCl_2 is very low at 32%RH at 20 °C (Kolthoff et al., 1969), so if the relative humidity is above the POD, at say 50%RH, salt crystals or salt solution will absorb water. If the relative humidity is below the POD, at say 20%RH, the solution will continue to evaporate and eventually form crystals.

Many common ionic solutions, such as sodium chloride (NaCl) and CaCl_2 , have the ability to attract water. Ionic solutions are often deposited onto mangroves (Lovelock et al., 2017), present in atmospheric particles (Burkhardt and Hunsche, 2013) and in sprinkler irrigation (Isla and Aragüés, 2009; Fernández et al., 2017). Small traces of additives such as NaCl , adjuvants, impurities and deposits on the leaf surface can significantly alter the POD of an ionic solution formulation by 4%RH to 17%RH, also changing the solutions maximum ion concentration (Chen and Lee, 2001; Fernández et al., 2017). We note the most important impact of a change in POD with an additive, applied to ionic AI penetration through plant leaves, is that more water can be absorbed, so the evaporation and penetration time is extended and hence there is more water available at the same relative humidity, increasing the area under the droplet and hence the number of aqueous pores available for penetration.

The effect of evaporation on AI penetration through plant cuticles is an important aspect to consider for both experimental and field work. Evaporation experiments on plant leaves are commonly performed at very low relative humidity (Zhou et al., 2017), below the POD, so do not account for hygroscopic water absorption. Theoretical evaporation models do not account for hygroscopic water absorption (Picknett and Bexon, 1977; Popov, 2005). We wish to model the deliquescent nature of ionic solutions, where the solutions can absorb water, as a function of any relative humidity and time. Evaporation can be simulated by considering a single sessile drop, deposited on a solid substrate, where the wetted area is characterized by a contact angle, contact radius and drop height, forming a spherical-cap shape (Erbil, 2012). Sessile droplet evaporation on a substrate is governed by the wettability and roughness of the substrate (Dash and Garimella, 2013), dictated by the contact radius and the contact angle of the droplet (Picknett and Bexon, 1977). These mechanisms are alternate to bulk solution evaporation (Tang et al., 1997) and a droplet suspended in air, which evaporates uniformly at a rate proportional to its radius (Dash and Garimella, 2013). The four general phases of partial wetting of an evaporating sessile drop, as shown in **Figure 1** [redrawn from Doganci et al. (2011); Semenov et al. (2013, 2014)], can be described as follows (Dash and Garimella, 2013; Semenov et al., 2013, 2014):

- 1) Spreading: A droplet is initially deposited on a surface and quickly spreads until an initial contact angle (θ_0) and radius ($r_{\text{drop},0}$) are reached. This phase occurs in under 2 min, for adjuvant solutions on leaf surfaces (Xu et al., 2011). Evaporation can be neglected here.
- 2) First Stage - Constant Contact Radius Mode: The first stage of evaporation, termed constant contact radius (CCR) mode, is characterized by a changing contact angle (θ) and a constant contact radius ($r_{\text{drop},0}$). The contact angle changes between the initial contact angle (θ_0) and the receding contact angle (θ_{rec}), which is found experimentally.

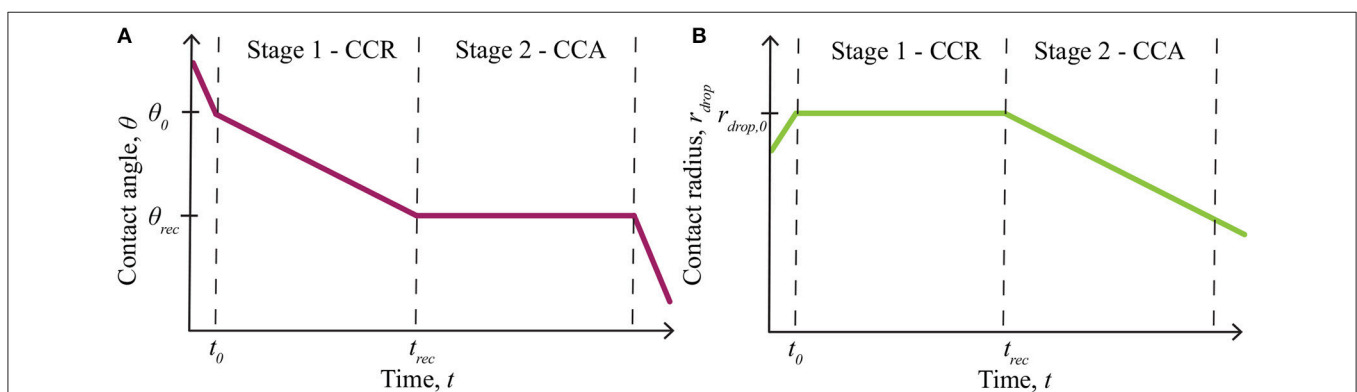


FIGURE 1 | Summary of evaporation modes, including the initial spreading phase and evaporation stages for partial wetting, redrawn from Doganci et al. (2011), Semenov et al. (2013, 2014). The contact angle change is shown in **(A)** and the contact radius in **(B)**. Only stage 1 - constant contact radius (CCR) and stage 2 - constant contact angle (CCA) mode, contribute to evaporation significantly. Evaporation starts at θ_0 and $r_{\text{drop},0}$, then the contact angle, θ , changes in stage 1, until it reaches θ_{rec} at t_{rec} . Stage 2 then begins, where the contact radius, r_{drop} , changes from $r_{\text{drop},0}$, until evaporation finishes. Reprinted (adapted) with permission from Semenov et al. (2013). Copyright 2013 American Chemical Society.

- 3) Second Stage - Constant Contact Angle Mode: The second stage of evaporation, termed constant contact angle (CCA) mode, is characterized by a constant contact angle (θ_{rec}) and a changing contact radius (r_{drop}).
- 4) Third Stage: The third and final stage of evaporation occurs over a short time and continues until the droplet completely evaporates. It is characterized by a changing contact angle and radius. This stage is usually ignored in evaporation models as it is relatively short.

In general, the first (CCR mode) and second (CCA mode) stages alone have been shown to govern evaporation, which has been confirmed both experimentally and theoretically (Semenov et al., 2013, 2014) and applies to a wide range of situations. This evaporation sequence has also been found to occur with RSO 5 (Hunsche and Noga, 2012). Dried deposit patterns of droplets of glyphosate with RSO 5 on various inorganic surfaces have been studied. Both the contact angle and radius changed during evaporation as both coffee-ring (CCR mode) and Marangoni flows (CCA mode) effects are shown along with other small island patterns. These effects change with surfactant concentration and type of surface (Hunsche and Noga, 2012).

A reliable, universally applicable, mechanistic mathematical model to simulate penetration of agrochemicals and adjuvants through plant cuticles would be beneficial as models aid to develop understanding of the governing mechanisms. Penetration experimental results are specific to each AI, formulation including adjuvant, plant species combination and environmental conditions including relative humidity. It has been noted that progress of agrochemical efficacy will not be made until appropriate models are created to simulate the multiple complex processes involved (Zabkiewicz, 2007). An interdisciplinary approach is needed in order to study these complex mechanisms.

Current mathematical models of penetration of ionic AIs have been created as alternatives to time consuming and expensive field/laboratory studies and fall into two categories: the first employ empirical expressions that require a rate constant to be measured specific to each different plant species, hydrophilic AI, adjuvant and environmental conditions (Forster et al., 2006; Schreiber and Schönherr, 2009, p. 132) and the second incorporate diffusion (Hsu, 1983; Satchivi et al., 2000; Veraverbeke et al., 2003; Mercer, 2007; Pecha et al., 2012). Comprehensive reviews can be found elsewhere (Forster et al., 2004; Trapp, 2004; Tredenick et al., 2017). These models, however, do not include important governing mechanisms such as ion binding, sessile droplet evaporation with water absorption including POD and relative humidity. The authors previously introduced a mechanistic mathematical model in Tredenick et al. (2017) to simulate ionic agrochemical penetration through plant cuticles with sessile droplet evaporation, the ability to vary plant species, type and initial concentration of active ingredient, relative humidity and ion binding. Adjuvants were not included and only a simplistic evaporation formulation was used, which did not consider the POD or water absorption of ionic AI

solutions. Here we wish to extend this model to include these mechanisms.

We aim to simulate the complex mechanisms involved in adjuvant enhanced hydrophilic ionic AI penetration through plant cuticles using a predictive mathematical model. This model will account for relative humidity, plant species variations and adjuvant effects. Specifically, we incorporate new mechanisms of water absorption, POD with evaporating droplets and effects of adding adjuvants such as the surfactant RSO 5. We seek to validate the predictions of our model against well-established experimental data and discuss the key implications of the models' sensitivities.

2. MODEL FRAMEWORK

The formulation of a mathematical model is based on an understanding of the experimental setup used. Here we will verify the solution of the model against well-established data from the experimental setup described in Kraemer et al. (2009), who studied the penetration of CaCl_2 and RSO 5 from droplets, applied to astomatous, isolated tomato fruit (*Solanum lycopersicum* L., cultivar "Panovy") cuticles. Droplets with known concentrations were applied to the adaxial cuticle surface. A receiver solution in a water bath was placed in close contact with the inner surface of the cuticle, which was analyzed at regular intervals for CaCl_2 . **Figure S1** shows the Kraemer et al. (2009) data for both CaCl_2 (A) and CaCl_2 with RSO 5 (B). We have presented their data as a mass percentage of the initial applied CaCl_2 , to further understand their results. The optimal way to visualize penetration results is as a mass percentage. We have fitted their data with a linear combination of exponential functions. Refer to the **Supplementary Materials** for further details. Two exponential terms were fitted to the data, which indicates there are at least two separate timescales involved in this penetration, governing at least two different mechanisms. In **Figure S1A** for CaCl_2 , the most important timescale is the first 5 h and penetration after this time occurs at a much slower rate. This rapid then slow penetration is well documented for ionic penetration through plant cuticles (Schönherr, 2006). **Figure S1A** shows that the mean percentage penetration for CaCl_2 is 40% at 48 h and penetration is not very sensitive to the initial concentration of AI (when the outlier 25 μg is excluded). This suggests that around 60% of AI has not been taken up through the cuticle. In **Figure S1B** for CaCl_2 with RSO 5, penetration is much higher than without RSO 5 (the mean penetration is 56.2% compared to 40% at 48 h). The mean percentage penetration was found to be 56.2% with a standard deviation of 8.4% at 48 h, hence the final penetration at 48 h is very similar across all initial concentrations. The penetration initially occurs rapidly, then levels off after 20 min.

Kraemer et al. (2009) have provided data for the initial droplet area, shown in **Table 1** for CaCl_2 and CaCl_2 with RSO 5. With spherical cap geometry, we can numerically approximate the initial contact angle, θ_0 , from the known initial droplet area and volume, the equation for $A_{drop,0}$ in **Table 2**, using the secant method (Wolfe, 1959). These values vary significantly

TABLE 1 | Initial droplet area from Kraemer et al. (2009), with varying CaCl₂ concentrations and RSO 5 addition.

Surfactant	Initial CaCl ₂ conc. (g/L)	Initial droplet area (m ²)	θ ₀ calculated	θ _{rec} calculated
None	1	0.49e-6	141.00	123.18
	5	0.84e-6	126.58	110.58
	10	0.86e-6	125.82	109.91
	15	0.57e-6	137.50	120.12
	30	0.55e-6	138.36	120.87
RSO 5	1	1.99e-6	87.91	76.79
	5	2.15e-6	83.32	72.79
	10	2.15e-6	83.32	72.79
	15	2.10e-6	84.73	74.02
	30	2.18e-6	82.48	72.06

with initial CaCl₂ concentration, with a nonlinear trend. The angle where CCA mode begins, termed the receding contact angle, θ_{rec}, is difficult to measure experimentally (Semenov et al., 2014). However, θ_{rec} can be estimated based on the behavior of experimental data with comparable initial contact angles (Stauber et al., 2015) and we find the contact angle should decrease by approximately 12.64%. Therefore, we reduce the values of θ₀ in **Table 1** by 12.64% to find θ_{rec}.

Crystallization of a solution of CaCl₂ will not occur at 20 °C if the relative humidity is above the POD as the solution will absorb water due to its hygroscopic nature (Dow Chemical Company, 2003). If the relative humidity is below the POD, evaporation will continue and the solution will eventually form crystals. Data published for the final solution weight percentage of CaCl₂ can be used to find the maximum concentration that CaCl₂ can reach before crystallization occurs as a function of relative humidity (Dow Chemical Company, 2003). This data can be fitted, as shown in **Figure 2A**, using the linear combination of two exponential functions:

$$c_{\text{mass}}(\Phi) = -0.8307 e^{3.618 \Phi} + 55.44 e^{-0.612 \Phi}, \quad (1)$$

where $c_{\text{mass}}\%$ is the final solution weight percentage of CaCl₂ as a function of the relative humidity adjustment factor, Φ. The advantage of fitting this data is that any relative humidity can be utilized.

The effect of relative humidity on water absorption over CaCl₂ at 25 °C has been studied (Dow Chemical Company, 2003). Data for the mass of water absorbed per mass of CaCl₂ applied (g_{H₂O}/g_{CaCl₂}) with relative humidity has been provided. Again, this data can be fitted using a linear combination of two exponential functions:

$$m_{\infty}(\Phi) = 0.307 e^{2.763 \Phi} + 1.218 \times 10^{-9} e^{24 \Phi}, \quad (2)$$

where m_{∞} is the equilibrium or maximum of the ratio of the mass of water absorbed per mass of CaCl₂ applied (g_{H₂O}/g_{CaCl₂}). **Figure 2B** shows the data fitted with Equation (2). The relative humidity has a large effect on water absorption over CaCl₂. In **Figure 2B** we can see that at high relative humidities, CaCl₂

absorbs very large volumes of water. At 95%RH, CaCl₂ can absorb 14 times its mass in water.

The POD of an ionic solution can change with the addition of an adjuvant (Chen and Lee, 2001; Fernández et al., 2017). If the POD of an ionic solution changes, the water absorption over the solution changes. As the POD of CaCl₂ with RSO 5 is unknown, we will assume RSO 5 changes the POD of CaCl₂ by 5%RH, similar to that found by Chen and Lee (2001). This changes the POD of CaCl₂ from 32%RH (Kolthoff et al., 1969) to 27%RH with RSO 5. The 5%RH change to the POD is referred to as ξ, and is a parameter that is easily altered within the model. When further research has been carried out in the future, this parameter can be modified.

With no surfactant, a relative humidity of 70%RH (Kraemer et al., 2009) is used to find $c_{\text{mass}}\%$ and m_{∞} . Fernández et al. (2017) found when the POD changed, so did the maximum solution concentration, $c_{\text{mass}}\%$. To find $c_{\text{mass}}\%$ and m_{∞} , in Equations (1–2), with the new POD, we assume a one-to-one relationship. When the POD is shifted with the addition of RSO 5, the value used to find $c_{\text{mass}}\%$ and m_{∞} , or the independent variable in Equations (1–2), Φ, is shifted from 70%RH to 75%RH.

If the POD is greater or equal to the relative humidity, $c_{\text{mass}}\%$ and m_{∞} are not included in the evaporation formulation. If the ionic AI or surfactant changes, producing a new POD, a new data set can be found experimentally, for $c_{\text{mass}}\%$ and m_{∞} , which can be fitted with a new function for $c_{\text{mass}}\%$ and m_{∞} .

2.1. Model Development

The model takes the form of a nonlinear, quasi-one-dimensional, diffusion model. We will briefly describe the modeling formulation, however we note that a full description can be found in the authors previous work (Tredenick et al., 2017). A schematic diagram of the model domain based on the experimental setup (Kraemer et al., 2009) is shown in **Figure 3**. Both AI and water diffuse and all variables change primarily along the cuticle membranes thickness, x ($0 \leq x \leq b$). In **Figure 3**, the initial condition is shown on the left (A) and a short time later on the right (B). In **Figure 3A**, initially a droplet with known initial contact angle, θ₀, radius, $r_{\text{drop},0}$, concentration of AI (CaCl₂), $c_{\text{AI},0}^{\text{drop}}$ and RSO 5 is placed on the outer cuticle surface, at $x = 0$. A well stirred water bath exists at the inner surface, at $x = b$. A single (for clarity) tortuous aqueous pore can be seen traversing the cuticle. In **Figure 3B**, after a short time later, some AI has diffused from the droplet into the cuticle toward the well stirred water bath. The droplet changes in size due to evaporation, hygroscopic effects and diffusion. Both the radius, r_{drop} , and contact angle, θ, of the droplet have changed. Ions of AI lost to ion binding can be seen as pink circles attached to the outer cuticle surface, which cannot diffuse. Adsorbed water is seen attached to the aqueous pore walls, shown as dark blue circles.

The model, including the variables and parameters as described in **Table 2** along with the governing partial differential equations, initial conditions (ICs), boundary conditions (BCs) and auxiliary functions, which is similar to previous work by the

TABLE 2 | Model parameters.

Parameter	Definition	Value and units	Comments
A_{Π}	Control volume area	m^2	
$A_{\text{drop}}(t)$	Drop surface contact area	m^2	Surface contact area of drop on cuticle surface, Erbil et al., 2002
$A_{\text{drop},0}$	Initial drop surface contact area on cuticle surface	m^2	$A_{\text{drop},0} = \pi^{1/3} (3g(\theta_0)V_0)^{2/3}$ Erbil et al., 2002
AI	Active ingredient		
b	Thickness of cuticle	$1.87e-5$ m	Chamel et al., 1991
$c_{\text{AI},0}^{\text{drop}}$	Concentration of AI in drop at $t = 0$	mol/m^3	Kraemer et al., 2009
$c_{\text{mass}\%}$	Solution weight percentage of CaCl_2	%	Refer to discussion around Figure 2A
$c_{\text{H}_2\text{O}}^{\text{pure}}$	Pure water concentration at 20°C and $t = 0$	$55,409.78 \text{ mol}/m^3$	calculated
c_{POD}	POD concentration	mol/m^3	Refer to discussion around Equation (31)
CCR	Constant contact radius evaporation mode		
CCA	Constant contact angle evaporation mode		
$c_i(x, t)$	Concentration of component i in plant cuticle	mol/m^3	
$D_{\text{AI}}^{\text{bulk}}$	Self/bulk diffusion coefficient of AI	$7.93e-10 \text{ m}^2/\text{s}$	For CaCl_2 , Ca^{2+} diffuses the slowest, so Ca^{2+} value is used, Yuan-Hui and Gregory, 1974
$D_{\text{H}_2\text{O}}^{\text{bulk}}$	Self/bulk diffusion coefficient of water	$2.299e-9 \text{ m}^2/\text{s}$	Holz et al., 2000
D_{evap}	Diffusivity of water in air	$2.4e-5 \text{ m}^2/\text{s}$	Semenov et al., 2013
$D_i(x, t)$	Diffusivity of component i	m^2/s	Liu and Nie, 2001
F_s	Fractal scaling dimension	1.203 (-)	$1 < F_s < 2$ (fitted)
$f(\theta)$	Functional variation of θ		Popov, 2005
$g(\theta)$	Functional of θ		Popov, 2005
H	Relative humidity	0.7 (70%)	Kraemer et al., 2009
i	Component AI (CaCl_2) or H_2O		
k	Ion binding reaction rate constant	$8.68e-16 \text{ m}^3/\text{s}$	(fitted)
L	Control volume length	1 m	
$M_{\text{w,H}_2\text{O}}$	Molecular weight H_2O	18.015 g/mol	
$M_{\text{w,AI}}$	Molecular weight of CaCl_2	110.98 g/mol	
m_{∞}	Equilibrium mass of water absorbed per CaCl_2 applied	$g_{\text{H}_2\text{O}}/g_{\text{AI}}$	Refer discussion around Figure 2A
N_A	Avogadro constant	$6.02214e23 \text{ mol}^{-1}$	
n_0	Number of aqueous pores on 1 m^2 of cuticle	(-)	Equals value of η_{pore}
P_V	Saturated water vapor pressure in air at 20°C	2338.8 Pa	Lide, 2004
POD	Point of deliquescence		$32\%RH$ for CaCl_2 Kolthoff et al., 1969 and $27\%RH$ for CaCl_2 with RSO 5
R	Gas constant	$8.3145 \text{ Pa}\cdot\text{m}^3/\text{K}/\text{mol}$	
RSO	Rapeseed oil surfactant		
r_{drop}	Drop contact radius	m	Contact radius of drop on cuticle surface
$r_{\text{drop},0}$	Initial contact radius of drop on cuticle surface	m	$r_{\text{drop},0} = (3g(\theta_0)V_0/\pi)^{1/3}$ Erbil et al., 2002
$r_{\text{H}_2\text{O}}$	Van der Waals radius of a water molecule	$1.5e-10$ m	Schreiber et al., 2006
$r_p(x, t)$	Radius of aqueous pore	m	
r_p^{max}	Maximum radius of aqueous pores	$2.12e-9$ m	For tomato fruit cuticle, (Schreiber and Schönherr, 2009, p. 87)
RH	Relative humidity in text		
t	Time	s	
T	Temperature	293.15 K (20°C)	Kraemer et al., 2009
u	dummy or bound integration variable		
V_0	Volume of droplet at $t = 0$	$1e-9 \text{ m}^3$	Kraemer et al., 2009
$V_{\text{H}_2\text{O}}^{\text{drop}}(t)$	Volume of water in droplet at time t		
$V_{\text{Del}}(t)$	Deliquescent droplet volume	m^3	
\bar{V}_{AI}	Partial molar volume CaCl_2	$1.6e-5 \text{ m}^3/\text{mol}$	Oakes et al., 1995
$\bar{V}_{\text{H}_2\text{O}}$	Partial molar volume water	$1.8047e-5 \text{ m}^3/\text{mol}$	Zen, 1957

(Continued)

TABLE 2 | Continued

Parameter	Definition	Value and units	Comments
x	Length	m	
β_{H_2O}	Langmuir parameter	$3.77e-5 \text{ m}^3/\text{mol}$	Equilibrium parameter of adsorbed water
$\varepsilon(x, t)$	Porosity of cuticle	(-)	$0 < \varepsilon < 1$
η_{pore}	Density of aqueous pores in cuticle	$2.18e15 \text{ m}^{-2}$	(fitted)
γ	Reduction factor for initial pore size	0.97	
$\Gamma_{H_2O}(x, t)$	Concentration of water adsorbed per unit area at equilibrium	mol/m^2	Luque et al., 1995; Bard and Faulkner, 2001
Γ_S	Langmuir saturation constant	$9.6832e-4 \text{ mol}/\text{m}^2$	$0 < \Gamma_{H_2O} < \Gamma_S$, saturation concentration of water adsorbed in aqueous pores per unit area
Λ	Evaporation constants as a function of relative humidity	m^2/s	$\Lambda = D_{\text{evap}} \psi / \rho_{H_2O}$ Erbil, 2012
$\psi(H)$	Saturated water vapor concentration as a function of relative humidity	g/m^3	$\psi = M_{w,H_2O} P_V(1 - H) / (R T)$ Erbil, 2012
Φ	Shifting factor for m_∞ and $c_{\text{mass}\%}$		
ρ_{H_2O}	Liquid density H_2O at 20°C	$9.98207e5 \text{ g}/\text{m}^3$	Weast and Lide, 1989
ρ_{Al}	Liquid density of CaCl_2 at 20°C	$2.16e6 \text{ g}/\text{m}^3$	Dow Chemical Company, 2003
$\theta(t)$	Contact angle of drop on cuticle surface that changes with time	rads	
θ_0	Contact angle of drop on cuticle surface at $t = 0$	rads	For CaCl_2 with RSO5, refer to Table 1
θ_{rec}	Receding contact angle of drop on cuticle surface	rads	Refer to Table 1
χ	Logistic decay evaporation constant	$0.043 \text{ L}^2/\text{g}^2$	(fitted)
$\bar{\chi}$	Logistic decay evaporation term (a constant) as a function of initial concentration of Al		calculated
ξ	POD shifting factor to incorporate with the addition of adjuvants	5%RH	

Dimensionless parameters are shown in the **Supplementary Materials**.

authors (Tredenick et al., 2017), is as follows:

$$\frac{\partial(\varepsilon c_{Al})}{\partial t} = -\frac{\partial}{\partial x} \left[-D_{Al} \frac{\partial(\varepsilon c_{Al})}{\partial x} \right], \quad 0 < x < b, t > 0, \quad (3)$$

$$\frac{\partial(\varepsilon c_{H_2O})}{\partial t} = -\frac{\partial}{\partial x} \left[-D_{H_2O} \frac{\partial(\varepsilon c_{H_2O})}{\partial x} \right] - \frac{2}{r_p} (1 - \varepsilon) \frac{\partial \Gamma_{H_2O}}{\partial t}, \quad 0 < x < b, t > 0, \quad (4)$$

$$\text{Functions: } r_p(x, t) = r_{H_2O} \left[1 + \left(\sin \left(\left(\Gamma_{H_2O} r_{H_2O}^2 N_A \right)^{-1} \right) \right)^{-1} \right], \quad 0 < x < b, t > 0, \quad (5)$$

$$\varepsilon(x, t) = \pi \left[\frac{r_p}{L} (\sqrt{n_0} + 1) \right]^2, \quad 0 < x < b, t > 0, \quad (6)$$

$$D_{Al}(x, t) = D_{Al}^{\text{bulk}} \varepsilon \left(\frac{F_s}{2 - F_s} \right), \quad 0 < x < b, t > 0, \quad (7)$$

$$D_{H_2O}(x, t) = D_{H_2O}^{\text{bulk}} \varepsilon \left(\frac{F_s}{2 - F_s} \right), \quad 0 < x < b, t > 0, \quad (8)$$

$$\Gamma_{H_2O}(x, t) = \frac{\Gamma_S \beta_{H_2O} c_{H_2O}}{1 + \beta_{H_2O} c_{H_2O}}, \quad 0 < x < b, t > 0, \quad (9)$$

$$\text{ICs: } c_{Al}(x, 0) = 0, \quad 0 < x < b, \quad (10)$$

$$c_{Al}(0, 0) = c_{Al,0}^{\text{drop}}, \quad (11)$$

$$r_p(x, 0) = r_p^{\text{max}} \gamma, \quad 0 \leq x \leq b \quad (12)$$

$$c_{H_2O}(x, 0) = c_{H_2O}^{\text{pure}}, \quad 0 < x < b, \quad (13)$$

$$c_{H_2O}(0, 0) = \frac{1 - \bar{v}_{Al} c_{Al}(0, 0)}{\bar{v}_{H_2O}}, \quad (14)$$

$$\Gamma_{H_2O}(x, 0) = \left(r_{H_2O}^2 N_A \arcsin \left(\left(\frac{r_p(x, 0)}{r_{H_2O}} - 1 \right)^{-1} \right) \right)^{-1}, \quad 0 < x < b, \quad (15)$$

$$\beta_{H_2O} = \left(c_{H_2O}(x, 0) \left[\frac{\Gamma_S}{\Gamma_{H_2O}(x, 0)} - 1 \right] \right)^{-1}, \quad 0 < x < b, \quad (16)$$

$$\text{BC - Al (bath): } c_{Al}(b, t) = 0, \quad t > 0, \quad (17)$$

$$\text{BC - H}_2\text{O (drop): } c_{H_2O}(0, t) = \frac{1 - \bar{v}_{Al} c_{Al}(0, t)}{\bar{v}_{H_2O}}, \quad t > 0, \quad (18)$$

$$\text{BC - H}_2\text{O (bath): } c_{H_2O}(b, t) = c_{H_2O}^{\text{pure}}, \quad t > 0. \quad (19)$$

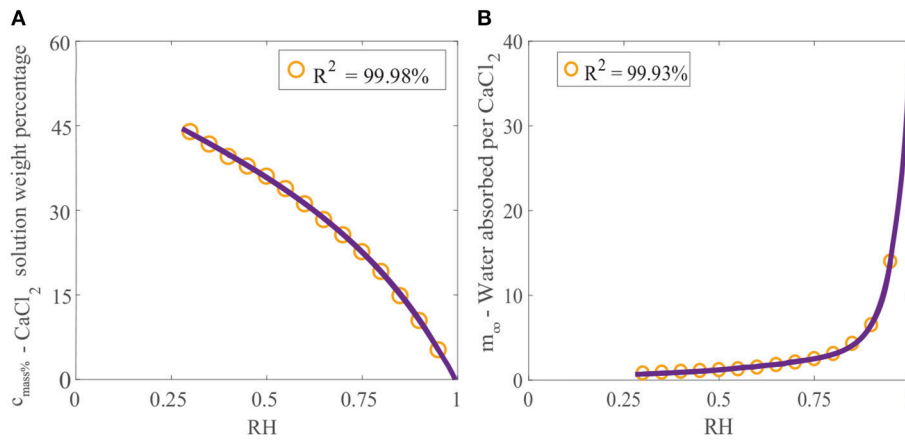


FIGURE 2 | (A) Effect of relative humidity on final solution weight percentage of CaCl_2 and **(B)** effect of relative humidity on water absorption over CaCl_2 (Dow Chemical Company, 2003). We have fitted the data, shown as the orange circles, with Equation (1) for $c_{\text{mass}\%}$, and Equation (2) for m_{∞} , shown as the purple line.

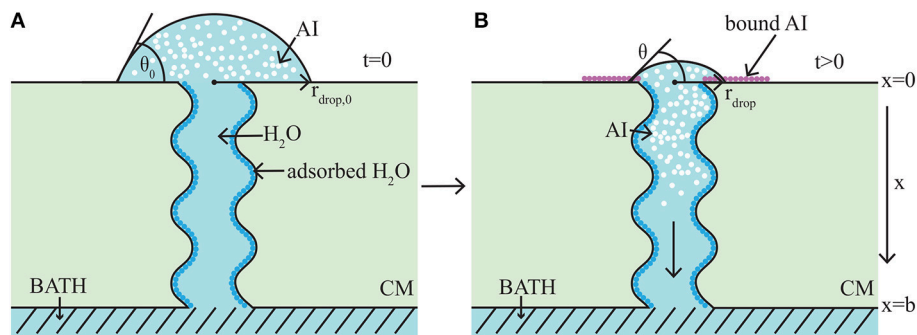


FIGURE 3 | 1-D cuticle model domain of AI diffusion and water adsorption-diffusion. The initial conditions of the model are shown on the left **(A)** and a short time later on the right **(B)**. Diffusion of AI starts at the outer surface (at $x = 0$), where a drop of solution containing AI and water having initial contact angle, θ_0 , and radius, $r_{\text{drop},0}$, sits. Over time AI travels through the porous cuticle membrane (CM) to the well stirred water bath at the inner surface (at $x = b$). Water adsorbs to the surface of the pore (shown as dark blue circles). In **(B)** at the cuticle surface (at $x = 0$), AI is trapped on the surface via ion binding, (shown as pink circles) and the droplet solution has undergone some evaporation and both the contact angle, θ , and radius, r_{drop} , have changed. For simplicity, a single tortuous aqueous pore can be seen crossing the cuticle (not to scale). Figure adapted from a figure published in Tredenick et al. (2017). The article was published under a Creative Commons CC-BY license.

The AI can travel through plant cuticle aqueous pores via Fickian diffusion (Equation 3), which depends on the swelling of aqueous pores due to adsorbed water molecules (Kerstiens, 2006; Schreiber and Schönherr, 2009). Water facilitates AI diffusion (Equation 4), by diffusing through aqueous pores first and opening up the pores by adsorption (Kerstiens, 2006). Both transport and reaction are nonlinear. Porosity limits diffusion through the cuticle and is based on the changing aqueous pore radius. It is necessary to model porosity as aqueous pores are known to change in size. Pores are assumed to be evenly distributed on the cuticle surface with circular cross sections. The number of pores on the area L^2 is given by $n_0 = \eta_{\text{pore}} L^2$. The model accounts for tortuous pores with diffusivities for AI and water that depend on both porosity and tortuosity described by the fractal scaling dimension (Equations 7–8) (Liu and Nie, 2001; Yuan and Sundén, 2014). The concentration of water molecules per unit area adsorbed as a monolayer to the aqueous pore walls is determined with a Langmuir isotherm (Equation 9) (Giles et al., 1974; Luque et al., 1995; Bard and Faulkner, 2001).

2.2. Initial Conditions

The initial conditions of the model are given in Equations (10–16). Equation (10) states there is no AI in the cuticle aqueous pores initially. Equation (11) states that there is initially a constant concentration of AI applied in the droplet solution, $c_{\text{AI},0}^{\text{drop}}$. The initial condition in Kraemer et al. (2009) for the aqueous pore size is somewhere between partially and fully swelled due to cuticle rehydration (author communication). We will assume the aqueous pores are initially at their maximum size, r_p^{max} . Equation (14) is simply Equation (18) at $t = 0$. The initial values for $\Gamma_{\text{H}_2\text{O}}$ and $\beta_{\text{H}_2\text{O}}$ in Equations (15) and (16) are found by rearranging Equations (5) and (9), and Γ_S can be found by assuming the pore radius is at its maximum when the pore surface is fully saturated and substituting $r_p = r_p^{\text{max}}$ and $\Gamma_{\text{H}_2\text{O}} = \Gamma_S$ into Equation (15).

2.3. Boundary Conditions

The BC for the concentration of AI at the bath is shown in Equation (17). The water bath is well stirred, so c_{AI} is zero.

Equation (18) is a conservation of volume statement for the concentration of water in the droplet, $c_{\text{H}_2\text{O}}$, based on the concentration of AI in the drop and the partial volume of AI and water, \bar{v}_{AI} and $\bar{v}_{\text{H}_2\text{O}}$. The mechanisms involved in penetration at the surface of the cuticle are important, so effects such as evaporation due to environmental conditions, hygroscopic water absorption and ion binding are incorporated. Only water evaporates from the drop. The AI concentration on the outer cuticle surface in the droplet is governed by:

$$\text{BC - AI (drop): } \quad \frac{d}{dt} \left(V_{\text{H}_2\text{O}}^{\text{drop}}(t) c_{\text{AI}}(0, t) \right) = -k c_{\text{AI}}(0, t) \\ + \eta_{\text{pore}} A_{\text{drop}}(t) A_{\Pi} \left[D_{\text{AI}}(x, t) \frac{\partial}{\partial x} (\varepsilon(x, t) c_{\text{AI}}(x, t)) \right] \Big|_{x=0}. \quad (20)$$

As water evaporates from the drop the concentration of AI in the drop, c_{AI} , increases (left hand side of Equation 20), then as the AI is transported from the drop into the cuticle (right hand side of equation) the concentration of AI in the drop decreases, governed by the circular cross sectional area of the control volume cylinder, A_{Π} , diffusivity of AI, D_{AI} , number of pores under the drop, $\eta_{\text{pore}} A_{\text{drop}}$, and porosity of the cuticle, ε . Ions are bound to the cuticle surface and trapped (Yamada et al., 1964), incorporated into Equation (20) using a reaction rate constant, k . If k is a non-zero number, the total percentage penetration of AI cannot reach 100%.

To account for the evaporation of a sessile droplet of an ionic AI and surfactant on a plant cuticle surface, we will assume evaporation occurs as the sequence of CCR mode followed by CCA mode. We will utilize the model described in Popov (2005) and expanded upon in Dash and Garimella (2013). The Popov (2005) quasi-steady sessile droplet evaporation model is an analytical diffusion model. It is valid over the entire range of contact angles ($0^\circ - 150^\circ$), and can be applied to superhydrophobic substrates. The initial droplet contact angle varies significantly between different plant species (Prüm et al., 2011; Delele et al., 2016). Therefore, the model can be applied to many physical situations such as the large variations in plant cuticle surfaces causing a wide range of initial contact angles. The Popov (2005) formulation assumes the droplet is sufficiently small so gravitational effects can be neglected. Zhou et al. (2017) have validated the Popov (2005) model with surfactant solutions on rice leaves. Evaporation is first governed by CCR mode, where the contact angle, θ , changes and the radius remains constant, $r_{\text{drop},0}$. CCR mode (Popov, 2005) is characterized by:

$$\text{CCR mode: } \quad \frac{d\theta}{dt} = \frac{-\Lambda (1 + \cos(\theta))^2 f(\theta)}{r_{\text{drop},0}^2}, \quad 0 < t \leq t_{\text{rec}}, \quad (21)$$

$$\frac{dV_{\text{H}_2\text{O}}^{\text{drop}}}{dt} = -\pi \Lambda r_{\text{drop},0} f(\theta), \quad 0 < t \leq t_{\text{rec}}. \quad (22)$$

To utilize the Popov (2005) model, the following auxiliary equations based on spherical-cap geometry (Picknett and Bexon,

1977; Erbil, 2012) are included:

$$g(\theta) = \frac{\sin^3(\theta)}{(1 - \cos(\theta))^2 (2 + \cos(\theta))}, \quad (23)$$

$$r_{\text{drop}}(t) = \left(\frac{3 g(\theta) V_{\text{H}_2\text{O}}^{\text{drop}}(t)}{\pi} \right)^{\frac{1}{3}}, \quad (24)$$

$$A_{\text{drop}}(t) = \pi^{\frac{1}{3}} \left(3 g(\theta) V_{\text{H}_2\text{O}}^{\text{drop}}(t) \right)^{\frac{2}{3}}, \quad (25) \\ \text{where } \theta(t).$$

The functional variation of the contact angle, $f(\theta)$, and the receding time, t_{rec} , which can be formulated by integrating Equation (21), are as follows (Popov, 2005):

$$f(\theta) = \tan\left(\frac{\theta}{2}\right) + 8 \int_0^\infty \cosh^2(\theta u) \operatorname{csch}(2\pi u) \tanh[(\pi - \theta) u] du. \quad (26)$$

$$t_{\text{rec}} = \int_{\theta_{\text{rec}}}^{\theta_0} \frac{r_{\text{drop},0}^2}{\Lambda (1 + \cos(\theta))^2 f(\theta)} d\theta. \quad (27)$$

If the relative humidity is above the POD, hygroscopic droplet growth will occur, therefore this effect needs to be included in a mechanistic model. A novel approach to a mechanistic evaporation model is to incorporate water absorption due to the hygroscopic nature of ionic AI solutions. We have formulated the following for CCA mode, where the radius, r_{drop} , changes and the contact angle is constant at θ_{rec} :

$$\text{CCA mode: } \quad \frac{dV_{\text{H}_2\text{O}}^{\text{drop}}}{dt} = -\pi \Lambda f(\theta_{\text{rec}}) \left(\frac{3 g(\theta_{\text{rec}}) V_{\text{H}_2\text{O}}^{\text{drop}}(t)}{\pi} \right)^{\frac{1}{3}} \\ \times \left[\frac{\bar{\chi}}{V_0} V_{\text{H}_2\text{O}}^{\text{drop}}(t) \left(\frac{V_{\text{H}_2\text{O}}^{\text{drop}}(t)}{V_{\text{Del}}(t)} - 1 \right) \right] \left(1 - \frac{c_{\text{AI}}(0, t)}{c_{\text{POD}}} \right) \\ + \frac{\eta_{\text{pore}} A_{\Pi} M_{\text{w,H}_2\text{O}} A_{\text{drop}}(t)}{\rho_{\text{H}_2\text{O}}} \left[D_{\text{H}_2\text{O}}(x, t) \frac{\partial}{\partial x} (\varepsilon(x, t) c_{\text{H}_2\text{O}}(x, t)) \right] \Big|_{x=0}, \\ H > \text{POD}, t > t_{\text{rec}}. \quad (28)$$

The first line of Equation (28) is derived in Popov (2005). The second and third lines of Equation (28) are explained as follows. The droplet volume, $V_{\text{H}_2\text{O}}^{\text{drop}}$, approaches the deliquescent droplet volume, V_{Del} . This volume, V_{Del} , is the minimum that the volume of water in the droplet, $V_{\text{H}_2\text{O}}^{\text{drop}}(t)$, can reach at a given point in time, POD and relative humidity. When the droplet volume, $V_{\text{H}_2\text{O}}^{\text{drop}}$, approaches V_{Del} , the evaporation rate tends to zero. This can be achieved with the addition of a logistic decay model. In Equation (28) this is achieved via the addition of a logistic decay term, namely,

$$\frac{\bar{\chi}}{V_0} V_{\text{H}_2\text{O}}^{\text{drop}}(t) \left(\frac{V_{\text{H}_2\text{O}}^{\text{drop}}(t)}{V_{\text{Del}}(t)} - 1 \right),$$

where $\bar{\chi}$ is a positive constant for logistic decay and describes the rate of maximum evaporation decrease and V_0 is the initial droplet volume,

$V_{\text{H}_2\text{O}}^{\text{drop}}$. At late times, $V_{\text{H}_2\text{O}}^{\text{drop}}$ approaches V_{Del} , but does not reach it due to the asymptotic nature of the logistic term. To prevent the concentration of AI going beyond c_{POD} , we multiply the evaporation formulation in Equation (28) by the term $(1 - c_{\text{AI}}/c_{\text{POD}})$. The logistic decay evaporation constant that multiplies the evaporation in Equation (28) is described as follows:

$$\bar{\chi} = \chi c_{\text{AI},0}^{\text{drop}^2}, \quad (29)$$

where $\bar{\chi}$ is the logistic decay evaporation term (a constant), χ is the logistic decay evaporation constant and $c_{\text{AI},0}^{\text{drop}}$ is the initial concentration of AI in the drop in g/L. The parameter $\bar{\chi}$ in Equation (29) was found to be a function of the initial concentration of the AI, as changing the initial concentration alters θ_0 (see **Table 1**).

The deliquescent droplet volume, V_{Del} , is the minimum value that the volume of water in the droplet, $V_{\text{H}_2\text{O}}^{\text{drop}}(t)$, can take at a given point in time, concentration of AI in the droplet, $c_{\text{AI}}(0, t)$, POD and relative humidity. We find V_{Del} with:

$$V_{\text{Del}}(t) = \frac{m_{\infty}(\Phi) M_{\text{w, AI}} c_{\text{AI}}(0, t) V_{\text{H}_2\text{O}}^{\text{drop}}(t)}{\rho_{\text{H}_2\text{O}}}, \quad t > 0, \quad (30)$$

where the deliquescent droplet volume, V_{Del} , is described by the mass ratio of water absorbed per mass of CaCl_2 applied, m_{∞} , the adjusted relative humidity, Φ , the molecular weight of AI, $M_{\text{w, AI}}$, the concentration of AI at the cuticle surface in the drop, $c_{\text{AI}}(0, t)$, the volume of water in the drop, $V_{\text{H}_2\text{O}}^{\text{drop}}(t)$ and the density of water, $\rho_{\text{H}_2\text{O}}$.

The maximum concentration of an ionic solution at a certain relative humidity and POD, c_{POD} , is modeled. Equation (1) for $c_{\text{mass}\%}$ can be used to find c_{POD} as follows:

$$c_{\text{POD}} = \frac{c_{\text{mass}\%}(\Phi) \rho_{\text{AI}}}{100\% M_{\text{w, AI}}}, \quad (31)$$

where c_{POD} is the maximum concentration that the AI can reach before crystallization occurs as a function of the shifted humidity, Φ , $c_{\text{mass}\%}$ is the final weight percentage of the AI, ρ_{AI} is the density of the AI and $M_{\text{w, AI}}$ is the molecular weight of the AI.

The concentration of water in the droplet can be less than in the cuticle. The concentration at the bath boundary condition for water is constant, as shown in Equation (19). This constant is the maximum value that the concentration of water can reach. If the concentration of water is less than pure water in the cuticle or cuticle surface, water will diffuse from regions of high to low concentration. At the cuticle surface boundary condition within the drop in Equation (18), the water concentration is slightly less than pure water due to the presence of AI. Diffusion of water can occur from the bath to the drop minutely, causing the droplet volume to increase. To account for this situation and conserve mass, an additional flux term for water is added, as seen in the third line of Equation (28). This term has the same constants as the flux term in the droplet boundary condition for AI in Equation (20), except the term is also converted to a volume in time by multiplying by the molecular weight of water, $M_{\text{w, H}_2\text{O}}$, and dividing by the density of water, $\rho_{\text{H}_2\text{O}}$.

If the relative humidity is below the POD of an AI with surfactant, the solution evaporates as follows:

$$\frac{dV_{\text{H}_2\text{O}}^{\text{drop}}}{dt} = -\pi \Lambda f(\theta_{\text{rec}}) \left(\frac{3 g(\theta_{\text{rec}}) V_{\text{H}_2\text{O}}^{\text{drop}}(t)}{\pi} \right)^{\frac{1}{3}} + \frac{\eta_{\text{pore}} A_{\Pi} M_{\text{w, H}_2\text{O}} A_{\text{drop}}(t)}{\rho_{\text{H}_2\text{O}}} \left[D_{\text{H}_2\text{O}}(x, t) \frac{\partial}{\partial x} (\varepsilon(x, t) c_{\text{H}_2\text{O}}(x, t)) \right] \Big|_{x=0}, \quad H \leq \text{POD}, t > t_{\text{rec}}, \quad (32)$$

which is the same as Equation (28), except it does not include hygroscopic growth.

To summarize, there are two parameters that changed within the model when RSO 5 is added. Firstly, the ξ adjustment factor, which alters the POD. It affects the maximum concentration AI can reach, c_{POD} and the maximum water absorption, m_{∞} , which impacts V_{Del} and evaporation rate. Secondly, the θ_0 , which changes the area of the drop, number of aqueous pores under the drop and evaporation rate - refer to **Table 1**. When the type or concentration of adjuvant is changed within the model, the following parameters change: ξ , θ_0 and scaling factor of 12.64% that used to calculate θ_{rec} from θ_0 , which impacts when the evaporation modes change.

2.4. Penetration Calculation

The output of our model is the concentration of AI, c_{AI} and water, $c_{\text{H}_2\text{O}}$, that has traveled through the cuticle to the water bath. Experiments measure penetration, which is the cumulative mass of AI in the water bath. We have formulated the penetration of calcium (Ca) as a mass, $m(t)$ (in μg), at the water bath as follows:

$$m(t) = -10^6 M_{\text{w, AI}} \eta_{\text{pore}} A_{\Pi} n_{\text{drops}} \times \int_0^{t_{\text{final}}} A_{\text{drop}}(t) \left(D_{\text{AI}}(x, t) \frac{\partial (\varepsilon(x, t) c_{\text{AI}}(x, t))}{\partial x} \right) \Big|_{x=b} dt, \quad (33)$$

where the constant 10^6 converts from g to μg and the flux at the bath boundary is integrated over time, where t_{final} is the experiment duration. We convert the mass penetration, $m(t)$, to a percentage as follows:

$$\% \text{ Ca penetration}(t) = \frac{m(t)}{10^9 c_{\text{AI},0}^{\text{drop}} n_{\text{drops}} V_0} \times 100\%, \quad (34)$$

where $m(t)$ is the mass penetration in μg from Equation (33), 10^9 converts from μg to g and m^3 to L, $c_{\text{AI},0}^{\text{drop}}$ is the initial applied concentration of AI in g/L, n_{drops} is the number of individual drops applied to the cuticle surface (5) and V_0 is the initial droplet volume in m^3 .

2.5. Dimensionless Model

The plant cuticle model as described in Equations (3 - 33) can be scaled and simplified using dimensionless parameters. This allows a sensitivity analysis to be performed, which is discussed in Section 3.1. For completeness, the full dimensionless model is shown in the **Supplementary Materials**.

2.6. Numerical Solution Procedure

The dimensionless model, as described in the **Supplementary Materials**, is solved numerically. This is achieved with a finite volume method by discretizing the model's partial differential

TABLE 3 | Comparison of the R-squared values for validation.

Surfactant	Figure	R-squared-%	Mean penetration-%	SD-%
RSO 5	Data	–	56.2	8.4
RSO 5	Figure 4	90.4	53.7	5.1
–	Data	–	41.8	5.7
–	Figure 5	83.6	32.6	4
Combined	Figures 4, 5	87	–	–

The mean mass percentage penetration at 48 h with standard deviation (SD) compared with experimental data (Kraemer et al., 2009) is also shown. All values without RSO 5 exclude the outlier (B) for 25 μg .

equations using second order central differences to approximate the spatial derivatives and averaging of the diffusivity function at the control volume faces with evenly distributed nodes (Grasselli and Pelinovsky, 2008, Chapter 6). The resulting system of ordinary differential equations is then solved using “ode15i” (Shampine, 2002) within MATLAB[®] (MATLAB, 2017) on a desktop computer. The parameters F_s , k , χ and η_{pore} were found by using optimization heuristics of a Nelder-Mead algorithm (Lagarias et al., 1998) with “fminsearch” and a Fedorov exchange algorithm (Fedorov, 1972), first with 5 μg , then across all five initial applied concentrations, for both CaCl_2 and CaCl_2 with RSO 5.

3. RESULTS

The dimensionless plant cuticle model, as described in the **Supplementary Materials**, is solved numerically. The fitting exercise provided a fit within the error bars of the experimental data across 10 graphs for both CaCl_2 , and CaCl_2 with RSO 5. The parameters are described in **Table 2**. We compare the numerical results of the CaCl_2 with RSO 5 model to the experimental data from Kraemer et al. (2009). All parameters used, F_s , η_{pore} , k and χ are the same across all 10 graphs, with the exception of the initial applied concentration of AI, $c_{\text{AI},0}^{\text{drop}}$. CaCl_2 is applied at 1, 5, 10, 15, and 30 g/L and each cuticle receives five 1 μL drops totaling 5, 25, 50, 75 or 150 μg of Ca per cuticle. The mean mass penetration at 48 h and mean R-squared values are shown in **Table 3**.

Figure 4 shows the validation of the CaCl_2 with RSO 5. In **Figure 4**, the numerical solution fits the data very well, as shown in **Table 3**, with the exception of **Figure 4E**. When comparing the mean mass penetration at 48 h, the numerical results compare very well. As seen in **Figure 4**, the penetration increases significantly over the first 10 h, then levels out and approaches a maximum value.

The mean percentage penetration at 48 h is 53.7% across all numerical solution results in **Figure 4**. As penetration has leveled out at less than 100%, it cannot increase further, unless an additional mechanism is identified. Penetration levels out due to the concentration of AI in the droplet reaching zero. Penetration levels out at less than 100% due to ion binding. In this case, ion binding causes 46% of the ions to be trapped, so is significant.

The fit in **Figure 4** is reasonable, with the exception of **Figure 4E** for 150 μg . Numerical tests reveal that this is largely due to the value of the ion binding term. When the parameters $F_s = 1.138$, $k = 3.74\text{e}^{-15}$, $\eta_{\text{pore}} = 1.99\text{e}15$ and $\chi = 0.0023$ are used, the fit improves. Across all 5 graphs with RSO 5, an R-squared value of 96.2% is obtained, including

the error bars. However, implementing this change over all 10 graphs including CaCl_2 alone does not improve the fit, so this parameter change is not retained.

Figure 5 is the validation of the numerical results of the model compared with data for CaCl_2 (without RSO 5). **Figure 5** produced a fit as seen in **Table 3**, excluding **Figure 5B**. **Figure 5B** is excluded as the total mean penetration for all the subfigures in **Figure 5** excluding **Figure 5B** is 42% with a standard deviation of 6%. However, in the experimental data of **Figure 5B**, the penetration is only 19%, so may be an outlier and no explanation is provided (Kraemer et al., 2009).

Overall, the validation of the plant cuticle model with CaCl_2 , and CaCl_2 with RSO 5 has produced reasonably good results, where one set of fitted parameters can produce fits over both data sets.

We note the experimental time is 48 h in **Figures 4, 5**. The numerical results for validation in these figures has been extended to 48 h for comparison with experimental data, while selected subsequent figures do not have the extended solution.

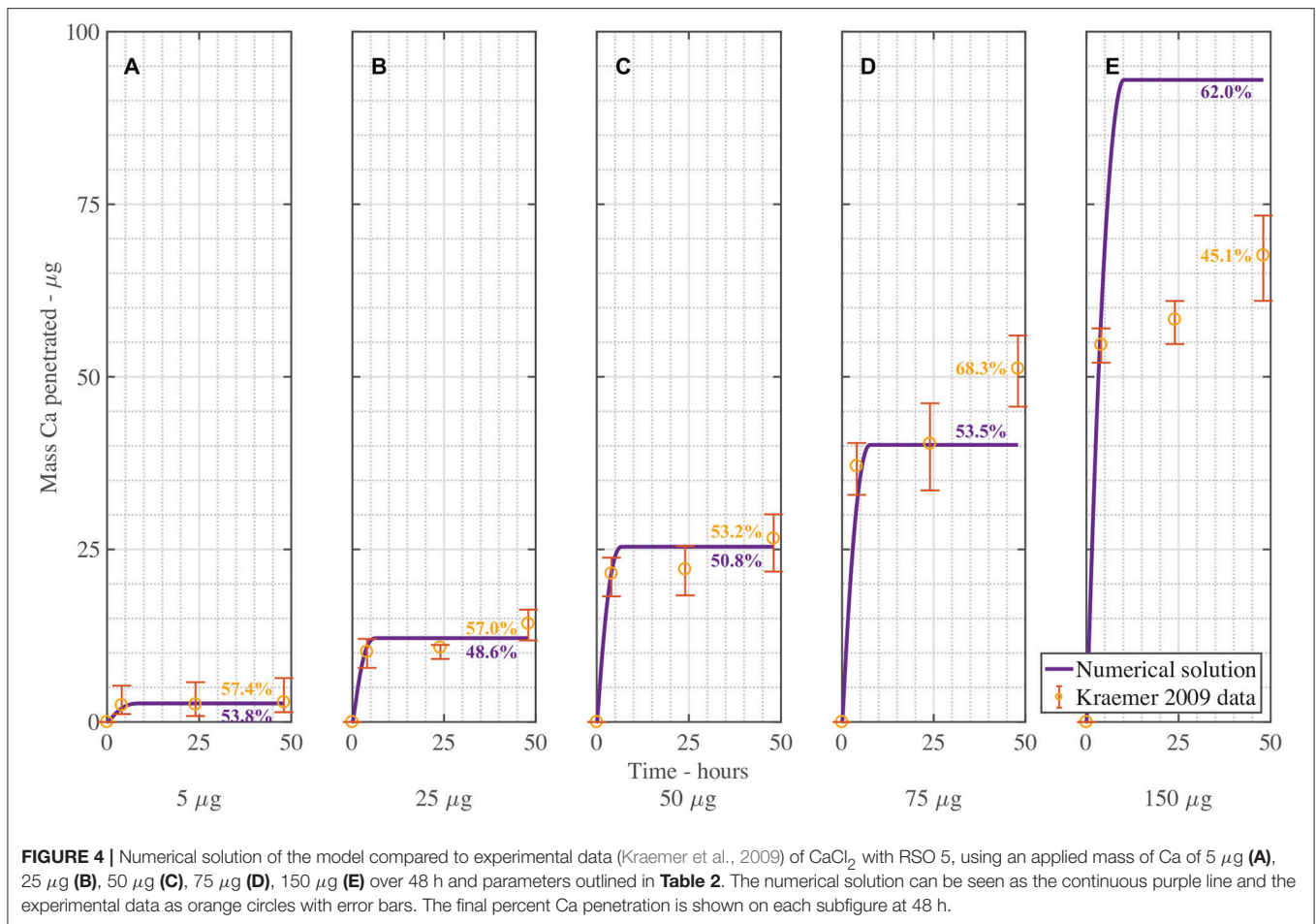
Figure S2 shows the results of AI diffusion and water diffusion with adsorption, through the plant cuticle in time. An initial concentration of AI of 1 g/L or 5 μg was used in both figures and parameters described in **Table 2**. The droplet of ionic solution is located at $x = 0$ and the water bath is located at $x = 1.87 \times 10^{-5}$ m. In **Figure S2A** we see the concentration profile of AI. The initial applied concentration of AI at the droplet, at $x = 0$, is 9 mol/m³, which quickly increases to 200 mol/m³ at 4.3 h, then decreases back to zero at 9.4 h. The initial rapid increase at the cuticle surface is due to the droplet solution becoming more concentrated due to rapid droplet evaporation in the first hour. Then the concentration of AI in the droplet decreases again as AI is transported into the cuticle via diffusion and ions are lost to ion binding. Within the cuticle aqueous pores, the AI is transported from regions of high concentration at the drop, to regions of low concentration at the bath, via diffusion.

Figure S2B shows the concentration profile of water. At the cuticle surface, the concentration of water in the droplet is inversely proportional to AI, as shown in Equation (18). The concentration of water at the droplet decreases further as the concentration of AI in the droplet increases due to evaporation. Then the water concentration increases again as AI concentration decreases and water diffuses in the direction from the bath to the water droplet. At late times equilibrium is reached and the concentration of water is that of pure water everywhere in the cuticle.

Figure 6 shows the numerical model results of a single initial applied concentration of AI of 9 mol/m³ and parameters shown in **Table 2**. The results are all shown at the droplet boundary condition, at $x = 0$, on the cuticle surface. **Figure 6A** shows the concentration of AI in the drop over time, $c_{\text{AI}}(0, t)$. Initially there is 9 mol/m³, then as time progresses, the concentration of AI in the droplet quickly increases due to rapid initial evaporation. The concentration then decreases as AI is transported through the cuticle via diffusion or is lost to ion binding over several hours.

Figure 6B shows the deliquescence droplet volume, V_{Del} over time. V_{Del} initially starts out at a large value as the initial droplet volume is large, then decreases as the water in the droplet, $V_{\text{H}_2\text{O}}^{\text{drop}}$, decreases.

Figure 6C shows the droplet contact angle, θ , over time. The evaporation starts in CCR mode, then continues in CCA mode. The contact angle changes from θ_0 to θ_{rec} . In **Figure 6C** we can see the change is not significant, as θ_{rec} is 12.64% less than θ_0 . The initial contact angle θ_0 is based on experimental data for the initial contact



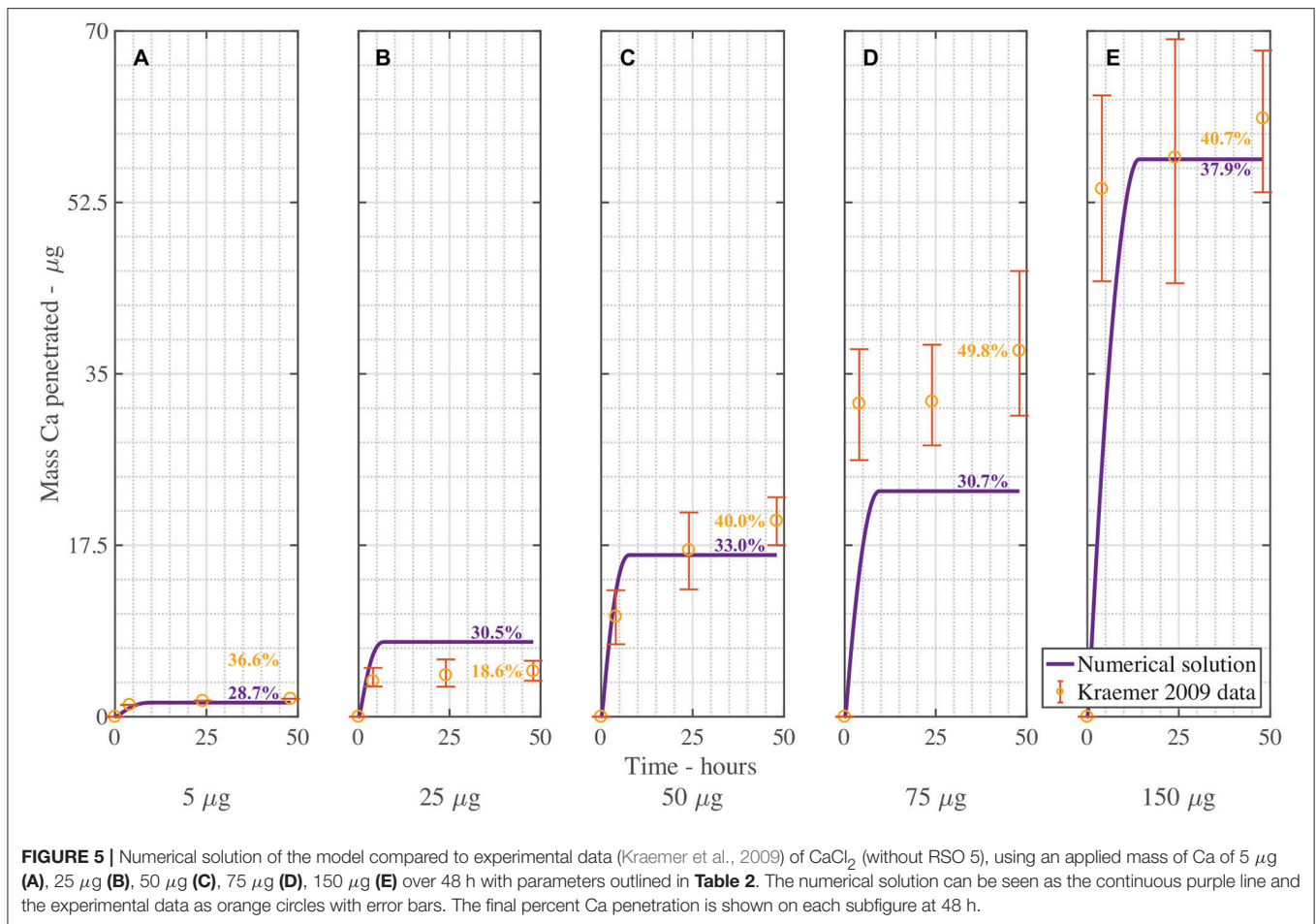
area, explained around Table 1. However, it is not clear at exactly what time the area was measured (initially or a few seconds or minutes later after droplet deposition). As discussed around Figure 1, the evaporation starts a few minutes after droplet deposition, when the spreading phase has ceased. Further experimental work could be carried out to explore the evaporation stages for CaCl₂ with RSO 5 on tomato fruit cuticles.

Figure 6D shows the volume of water in the droplet, $V_{\text{H}_2\text{O}}^{\text{drop}}$, over time. The evaporation is initially rapid over the first hour, then after 1 h, the evaporation rate has reduced due to water absorption and POD effects governing the equation. The evaporation rate continues to reduce smoothly and the droplet completely evaporates at 9.4 h. Without the input of hygroscopic water absorption in the droplet, numerical tests show the drop would completely evaporate at 40 min and penetration would cease as there is no water in the droplet. Therefore, the water absorption effects have promoted a significant extension to the penetration timescale from 40 min to 9.4 h, allowing further penetration through the cuticle.

Figure 6E shows the droplet radius, r_{drop} , over time. After the model has been solved numerically, the droplet volume, $V_{\text{H}_2\text{O}}^{\text{drop}}$, and contact angle, θ , are known. The droplet radius can then be calculated with Equation (24) to plot Figure 6E. As the evaporation mode starts at CCR mode, the radius is initially constant, then evaporation continues as CCA mode until the droplet completely evaporates and

the radius decreases until penetration ceases. This change in the droplet radius is dictated by the droplet volume from Equation (28). Figure 6F shows the percentage mass penetration over time. Here we can see penetration is rapid over the first 5 h, then after 5 h, the penetration rate decreases and ceases at 9.4 h.

Figure 7 shows the results of the change in the droplet profile, over time. The sessile droplet with a spherical cap geometry sits on the outer cuticle surface (black line). When the model is solved numerically, the droplet radius and contact angle are known at every point in time. The droplet can then be plotted using spherical cap geometry. The radius of the whole sphere containing the spherical cap, $R_s = r_{\text{drop}}/\sin(\theta)$ (Erbil, 2012) and θ are converted to polar coordinates and plotted. In Figure 7, initially a drop with an initial contact angle, θ_0 , and radius, $r_{\text{drop},0}$, sits. The drop then evaporates in CCR mode until t_{rec} is reached at 0.11 h, where we can see the angle has changed but not the radius. Then the evaporation mode changes to CCA mode where the radius changes but the contact angle stays constant. The droplet radius rapidly decrease over the first hour. Then to 9.3 h, evaporation reduces significantly due to hygroscopic effects. At around 9.4 h, the droplet has completely evaporated. This figure shows the evaporation modes and the impact the area under the drop has, which is changing in time. There is a substantial decrease in the area under the drop and consequently the number of aqueous pores under the drop in the first hour, which reduces the penetration rate.



3.1. Sensitivity Analysis

A sensitivity analysis was performed with the results from the dimensionless model. We have used values for CaCl_2 with RSO 5 given in Table 2 with $c_{\text{AI},0}^{\text{drop}} = 1 \text{ g/L}$. The one-factor-at-a-time method has been utilized to determine parameter sensitivity (Saltelli et al., 2008). A selection of parameters having the highest to lowest effect on percentage penetration are shown in Table 4. Further details can be found in Supplementary Materials Section 4 and Tredenick et al. (2017). A selection of sensitivities are discussed below.

3.1.1. Fractal Scaling Dimension and Relative Humidity - F_s and H

The fractal scaling dimension for the tortuosity of the aqueous pores, F_s , influences penetration to an extremely high level, as shown in Table 4 and Figure 8A. In Figures 8, 9, the reference case, used for validation, can be seen in purple and the experimental data as green circles. In the model, F_s impacts the effective diffusivity of the AI and water. As seen in Figure 8A, changing F_s alters the timescale of penetration. At a F_s of 1, penetration can rapidly reach 90%, while at F_s of 1.9, penetration is close to zero. In isolated cuticles, the tortuosity of the aqueous pores will vary between plant species to a significant degree due to structural changes like lamellate structures, thickness, orientation of pores and plant age (Santier and Chamel, 1992; Schreiber et al., 2006; Jeffree, 2008; Kerstiens, 2010). The large effect F_s has over penetration may explain the differences seen

in penetration in different plant species, which is consistent with experimental work (Schreiber et al., 2006).

In Figure 8B we can see the sensitivity of our model to the relative humidity, H . As humidity increases, the maximum percentage penetration also increases and is highly influential over penetration, as seen in Table 4. Relative humidity changes the timescale of penetration. In the model, relative humidity affects penetration by influencing the evaporation rate, the POD, the maximum concentration of the solution and the water absorption over the AI.

In Figure 8B, at high humidities, such as 90%RH or 97%RH, the highest penetration is obtained. High relative humidity promotes high penetration as the droplet evaporates at a slower rate, hence the droplet is larger, covering a larger surface area and hence a larger number of pores under the droplet, extending the penetration time.

When relative humidity is close to saturation at 97%RH, 84% penetration is achieved. As penetration has leveled out and ceased at less than 100% penetration, this indicates some ions are lost to ion binding (16%), but less than at 70%RH (45% loss to ion binding). This is due to a linear relationship with the concentration of AI in the droplet in Equation (20). At high humidities, the droplet stays dilute for longer as the evaporation rate is reduced, so less ions are lost to ion binding. This indicates there is a balance that needs to be found between humidity and concentration of AI in the droplet.

In Figure 8B, the lowest penetration is obtained at 25%RH, reaching 2% at 16 min. The POD_{AI} of CaCl_2 is 32%RH, which is

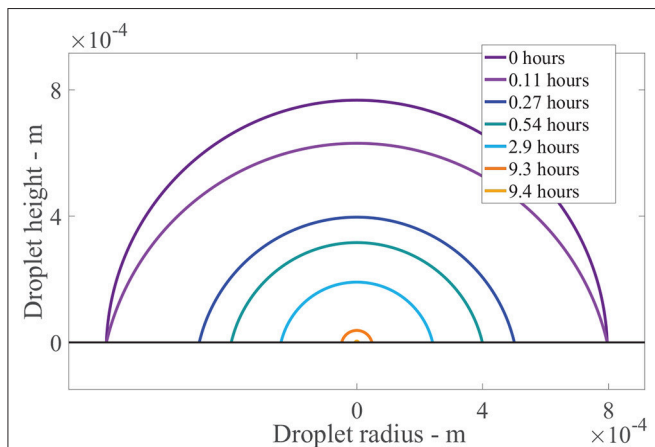
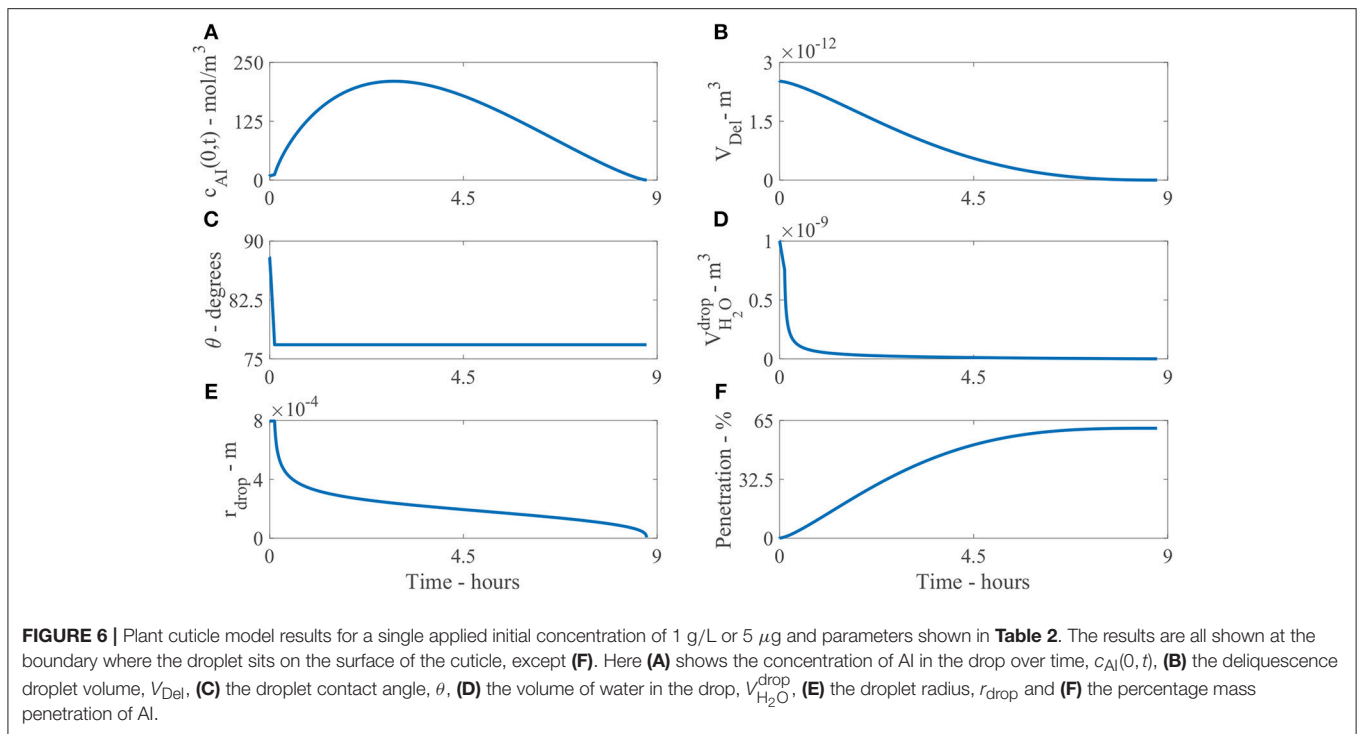


FIGURE 7 | Droplet evaporation profile results for the plant cuticle model. An evaporating sessile droplet of a spherical cap shape are shown as a cross-section, changing in time, on the cuticle surface. A single applied initial concentration of 1 g/L or 5 μg is used and parameters shown in **Table 2**. The cuticle surface is shown as the horizontal black line. The radius of the drop and droplet height are shown in meters.

above the humidity of 25%RH, which means AI does not absorb water and the droplet evaporates according to Equation (32). The penetration ceases when there is no water left on the cuticle surface or the concentration of AI is zero. The water evaporates very quickly as the evaporation rate has increased due to the low relative humidity and there is no water absorption. This has caused penetration to end at 16 min compared to 35 h with 97%RH and much lower penetration. Relative humidity has a significant impact and shows the importance of the POD.

In isolated cuticles, penetration has been found to increase significantly with relative humidity (Schönherr, 2000, 2002). In **Figure 8B** this significant increase is also seen, where penetration increases exponentially as relative humidity increases. The cause of this increase is due to the exponential increase in hygroscopic water absorption over the CaCl_2 , as seen in **Figure 2B**. At high relative humidities, the water absorption is very high, which produces high penetration in **Figure 8B**. Several studies have investigated ionic AI penetration with adjuvants under various relative humidities through isolated cuticles but are rarely with RSO 5. These studies are worth considering nonetheless. Several studies have shown relative humidity has a significant impact on penetration with and without adjuvants and is directly proportional (Middleton and Sanderson, 1965; Schönherr, 2000, 2002, 2006). These results indicate our model has the potential to predict changes in relative humidity, beyond the Kraemer et al. (2009) data and are in line with the well-established literature.

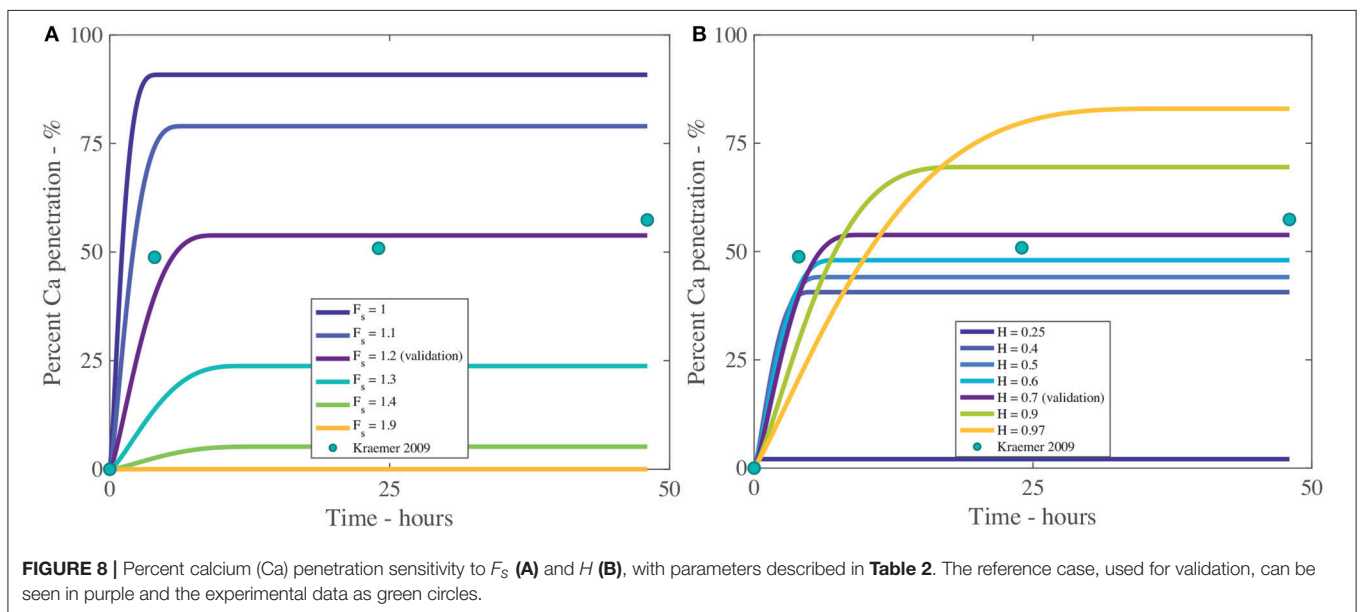
3.1.2. Initial Droplet Contact Angle and Initial Droplet Volume - θ_0 and V_0

The effect that the initial contact angle, θ_0 , has on penetration can be seen in **Figure 9A** and **Table 4**. The sensitivity analysis reveals that θ_0 is highly influential over penetration, having an inverse relationship to penetration. Within the model, θ_0 has the most influence over penetration by changing the initial contact area under the droplet, which changes the number of pores available to diffusion. Decreasing the contact angle is one way surfactants influence the droplet. In **Figure 9A**, penetration still increases with decreasing initial contact angle, despite this decreased penetration time and increased evaporation rate, due to the balance that is obtained by increasing the droplet contact area, the number of pores under the drop and the AI in the droplet becoming more concentrated earlier,

TABLE 4 | Sensitivity rankings of parameters based on the one-factor-at-a-time method, calculated in 3 ways - percentage relative sensitivity at the final time (48 h), $S_{\%}$, and the sensitivity based on the residual sum of squares, SS_{res} and root-mean-square error, RMSE over time, $S_{SS_{res}}$ and S_{RMSE} .

Parameter	Description	$S_{\%}$	$S_{SS_{res}}$	S_{RMSE}	Proportionality
F_s	Fractal scaling - tortuosity	1	1	1	Inverse
r_p^{max}	Maximum aqueous pore radius	2	2	2	Direct
H	Relative humidity	3	4	3	Direct
η_{pore}	Aqueous pore density	4	3	4	Direct
ξ	POD RH adjustment factor for RSO 5	5	6	6	Direct
θ_0	Initial droplet contact angle	6	5	5	Inverse
k	Ion binding	7	8	8	Inverse
b	Cuticle thickness	8	7	7	Inverse
χ	Droplet evaporation scaling factor	9	9	9/10	Inverse
V_0	Initial droplet volume	10	10	9/10	-
$c_{AI,0}^{drop}$	Initial AI droplet concentration	11	11	11	-

Additional details can be found in **Supplementary Materials** section 4.



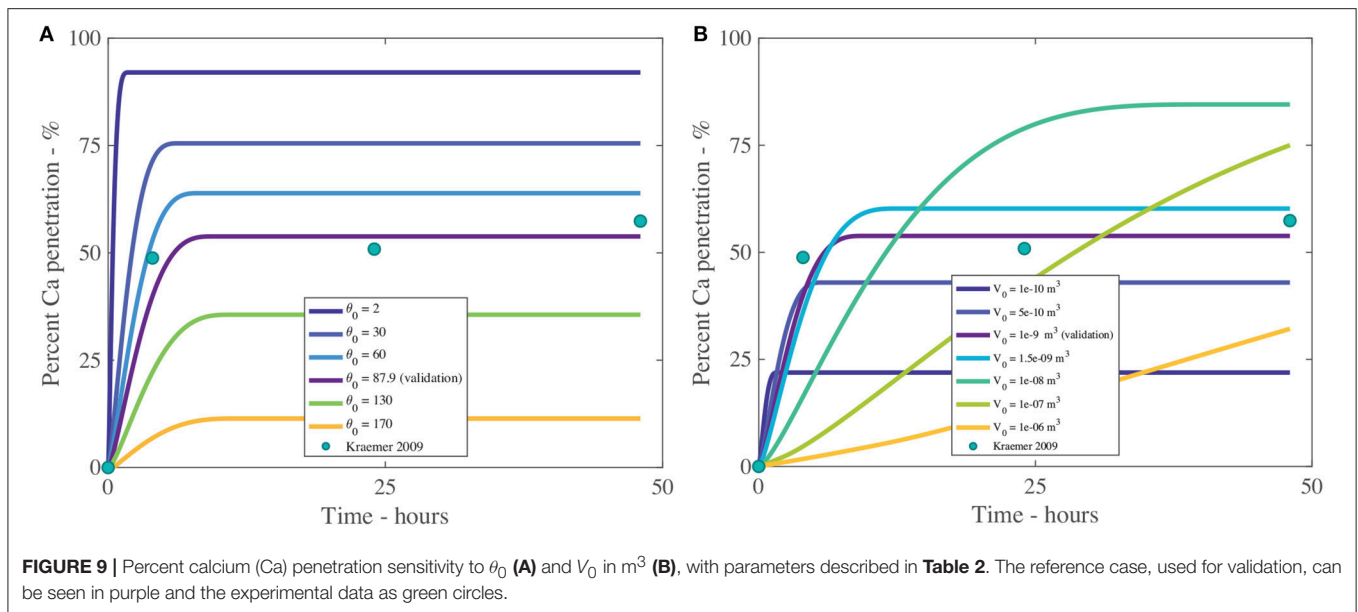
promoting penetration. This increased evaporation rate of low flat drops produced using surfactants is also seen in the literature, where a thinner liquid layer is created. This thin layer promotes heat transfer from the solid to the liquid-vapor interface. The contact area of the droplet also increases the heat transfer area. These two effects promote surface cooling, which promotes droplet evaporation (Chandra et al., 1996).

The initial contact angle changes with type and concentration of adjuvant (Haefs et al., 2002; Xu et al., 2011) and plant species. Some plant species are easy to wet while others are difficult to wet, based on surface structures such as trichomes, stomata and cuticle folds. Here the results of the sensitivity analysis align with the well-established literature and allow for the inclusion of many different plant species and adjuvant into the model.

The initial volume of the droplet, V_0 , as shown in **Figure 9B** and **Table 4**, has a large impact over penetration. We note only V_0 has changed, not the initial contact angle or initial concentration of AI. The initial droplet radius and area, which are calculated,

do change. In **Figure 9B**, we can see that increasing the initial volume increases percentage penetration and alters the timescale of penetration. However, at large volumes, the penetration is not as high. In **Figure 9B**, a V_0 of $1 \times 10^{-8} \text{ m}^3$ reaches 90% penetration quickly and seems to be the optimal value here. In **Figure 9B**, we can see that a small initial volume of $1 \times 10^{-10} \text{ m}^3$ reaches 20% penetration and ceases very quickly. The droplet is so small that evaporation is very rapid. This causes the droplet to become concentrated very quickly, which increases the concentration gradient through the cuticle, promoting rapid penetration and ion binding.

An initial volume of $1 \times 10^{-6} \text{ m}^3$ is the largest value tested, however it has not yet reached its maximum penetration. If the timescale is increased to 150 h, close to 100% penetration is obtained using the two largest initial volumes. It would appear that there is a balance that needs to be achieved with the initial droplet volume. Evaporation will be much slower for a larger droplet and it will become highly concentrated at a much later time. A balance needs to be



found where the droplet is small enough to cause some evaporation and increased droplet concentration, but not too small otherwise the evaporation is too rapid and penetration quickly ends.

When the initial volumes are applied to sprays, they correspond to spherical droplets in air of diameters of 600, 980, 1,400, 2,600, 6,000, and 12,400 μm . Sprays are typically 60–600 μm and large rain is up to 4,000 μm (ASABE, 2009), so the two largest volumes in Figure 9B are unlikely to exist in nature.

In isolated cuticles, the low penetration with a large droplet size and the balance that needs to be found could possibly explain why certain ionic AIs such as glyphosate can require a concentrated droplet to promote penetration. Santier and Chamel (1992) studied glyphosate (without adjuvants) through isolated tomato fruit cuticles and found that at 100%RH, penetration does not occur until after 20 h when the droplet has mostly evaporated, then penetration can reach 90%.

3.1.3. Point of Deliquescence

We investigate the sensitivity of the model to the point of deliquescence, POD. We investigate the POD of other possible ionic AIs. We note that the water absorption data for other ionic AIs, $c_{\text{mass}\%}$ and m_{∞} , would vary. When the ionic AI or surfactant changes, producing a new POD, new experimental data can be found for $c_{\text{mass}\%}$ and m_{∞} , which can then be fitted with a function.

To find the POD of an ionic AI solution with a surfactant, we consider how much change this has applied to the POD of the ionic AI solution. Here we consider large changes to the POD, so large values of ξ , the POD adjustment factor, as seen in Table S1. To then find the resulting values for $c_{\text{mass}\%}$ and m_{∞} , we find the value of the independent variable, Φ , which is based on the relative humidity, H , the change in POD, ξ , and the ionic AI solution POD without surfactant, POD_{AI} (32%RH for CaCl_2 Kolthoff et al., 1969), as follows:

$$\Phi = \begin{cases} H + \xi & : H + \xi > \text{POD}_{\text{AI}}, \\ 97\% & : H + \xi > 97\%. \end{cases} \quad (35)$$

In Equation (35), if $H + \xi$ is larger than POD_{AI} , water absorption can occur. If $H + \xi$ is larger than 97%RH, Φ is set to 97%RH. If

$H + \xi$ is less than or equal to POD_{AI} , $c_{\text{mass}\%}$ and m_{∞} are not included in evaporation and penetration ceases when there is no water in the droplet or the concentration of AI has reached zero.

We have investigated 3 different relative humidities with 3 different POD values for each, as shown Figure 10. In Figure 10A, at a low relative humidity of 33%RH, only a very low POD of 5%RH can allow water absorption and hence increased penetration to occur, reaching 40% penetration at 5 h. The penetration at a POD of 5%RH is 19-fold that of the penetration at a POD of 62%RH and 97%RH at the final time or a relative change of 44%. In Figure 10B, at 70%RH, higher water absorption is attainable, increasing final penetration time and penetration. The highest penetration is 13-fold that of the lowest or a relative change of 68%. The effect is similar in Figure 10C, at 90%RH, where the highest penetration is 4-fold that of the lowest or a relative change of 63%. Figures 10A–C shows the significant effect POD with relative humidity has on penetration and is a significant limiting factor, with a 19-fold difference in some cases. In isolated cuticles, we surmise this POD limiting factor is one of the reasons very low penetration is seen in some cases without adjuvants (Santier and Chamel, 1992), significantly limiting penetration.

3.1.4. Other Parameters - η_{pore} , b , $c_{\text{AI},0}^{\text{drop}}$, ξ

The aqueous pore density, η_{pore} , controls the porosity of the cuticle. As seen in Table 4, the pore density is very highly influential over penetration, it changes the timescale of penetration and is directly proportional. The parameter η_{pore} would change when plant species is changed or perhaps growing conditions (Karbulková et al., 2008) or leaf age (Viougeas et al., 1995).

The thickness of the cuticle, b , is highly influential over penetration, changes the timescale of penetration and is inversely proportional. The thickness of the cuticle alone is changed and the remaining characteristics of the cuticle remain the same, so the tortuosity and pore radius remain the same, therefore the diffusion path length is increased (Riederer and Schreiber, 1995), which decreases penetration. Changing cuticle thickness is one way to incorporate plant species variation. Ionic AIs take longer to diffuse

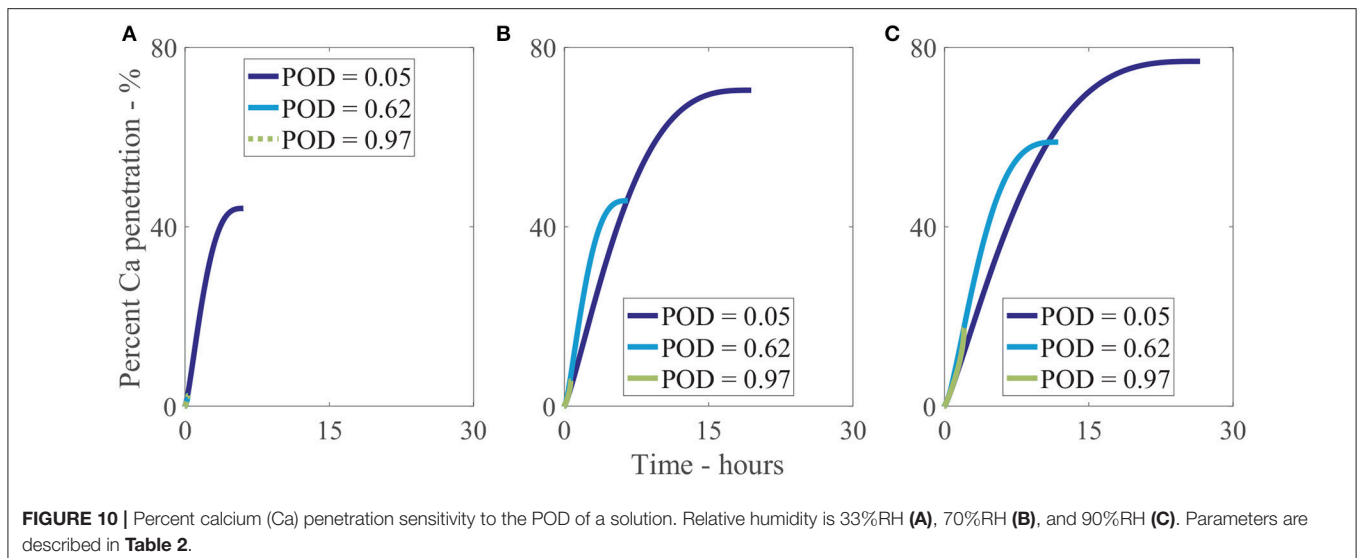


FIGURE 10 | Percent calcium (Ca) penetration sensitivity to the POD of a solution. Relative humidity is 33%RH (A), 70%RH (B), and 90%RH (C). Parameters are described in Table 2.

through the pores of thicker cuticles, which is supported by the literature (Santier and Chamel, 1992). The inverse proportionality and sensitivity of cuticle thickness is in line with the well-established literature.

The initial concentration of AI, $c_{AI,0}^{drop}$, has moderate impact over the penetration as seen in Table 4. The proportionality of $c_{AI,0}^{drop}$ over penetration is nonlinear, as it influences many aspects within the model. Changing $c_{AI,0}^{drop}$ leads to choosing an alternative θ_0 , as shown in Table 1. In isolated cuticles, the penetration of $CaCl_2$ with and without adjuvants has been shown to have only a slight dependence on the initial concentration of $CaCl_2$ (Schönherr, 2000; Kraemer et al., 2009). Penetration in isolated astomatous *Pyrus* cuticles, at 90%RH, with an initial concentration of $CaCl_2$ of 1 g/L, 2 g/L, 4 g/L and 6 g/L (with 0.2 g/L Glucopon 215 CSUP as a wetting agent) produced around 95% penetration at 100 h (Schönherr, 2000), therefore having no sensitivity to the initial $CaCl_2$ concentration. The results for the initial concentration of AI align with the well-established literature.

The POD shifting parameter, ξ , describes how the POD of a solution and the relative humidity have changed with the addition of an adjuvant. We investigate this to show the model can accommodate changes in POD of ionic solutions. As shown in Table 4, ξ has a high effect over penetration and is directly proportional to penetration. When the POD is below the relative humidity, water absorption can occur over AI in the droplet due to hygroscopic effects. When the POD is above the relative humidity, penetration may be limited as water absorption is not included in the model.

To summarize, the parameters that are highly influential over penetration are related to variations in plant species. These parameters include θ_0 , r_p^{max} , η_{pore} , b , F_s and k . This parameter combination could perhaps explain the significant differences in penetration that is seen in experimental work (Schreiber et al., 2006) in isolated cuticles from different plant species.

Parameters that impact the evaporation rate of H , θ_0 , V_0 , χ , POD and ξ impact penetration to a significant degree. However, this collective effect is less than that of the plant species parameters.

The individual parameters that have the most effect over penetration within the sensitivity analysis are the tortuosity, F_s and the maximum pore radius, r_p^{max} . This indicates cuticle structure plays the most influential role over penetration. Relative humidity, H , and pore

density, η_{pore} , also significantly impact penetration. The ion binding, k , relative humidity, H , POD adjustment factor, ξ , and POD were found to be limiters to penetration. There is an optimal value that needs to be found to obtain adequate penetration.

When changing the model between fitting $CaCl_2$ with and without RSO 5, two parameters changed, ξ , which alters the POD of the solution and the water absorption of the ionic droplet solution and θ_0 . These parameters influence many interconnected aspects of the model. A 5% change of ξ has a minimal effect on penetration. Numerical analysis shows that the most significant impact of changing θ_0 , is that it varies the initial droplet contact area and the number of pores under the droplet. When including RSO 5, the initial droplet area is much larger. Then as time progresses, the area under the droplet remains much larger than without RSO 5, as the volume changes at a similar rate. The rate of evaporation is only slightly different with and without RSO 5. The area of the drop influences the rate that the AI travels into the cuticle in Equation (20) and the AI penetration in Equation (33). Therefore RSO 5 increases penetration in this case due to the change in θ_0 and the number of pores under the drop.

The sensitivity analysis has provided some insight into why surfactants in general increase penetration. We can see from the sensitivity results for ξ and the POD, that if an AI has very little penetration without surfactant, when a surfactant is added it significantly alters the POD of the solution and penetration can increase significantly. Changing the POD of a solution will allow more water to be absorbed at lower relative humidities and delay evaporation, which increases the droplet spread area, the number of pores under the droplet and extends the penetration timescale, which increases penetration. Changing θ_0 also increases penetration as shown in Figure 9. We surmise the effect that surfactants have of changing a solutions POD, which significantly increasing penetration, could partially explain the large increase in penetration found in some isolated cuticle experiments (Coret and Chamel, 1993; Schönherr, 2000).

4. DISCUSSION

We have numerically solved our plant cuticle diffusion model and produced results, further discussed here. The model has 4 fitted

parameters, F_s , k , χ , and η_{pore} , as described in **Table 2**. We will discuss the implications of the value of these parameters.

From the fitting exercise, a low value for the fractal scaling dimension (for tortuosity), F_s , was obtained. This indicates the tortuosity of the aqueous pores in tomato fruit cuticles is in the lower range of tortuosity (tending to straight). Penetration is quite rapid, so this is logical. If a higher value for F_s was used, for example, 1.7, this would indicate very tortuous pores and penetration would be slow. If a certain plant species has a low diffusivity, very tortuous pores, a highly lamellate cuticle structure or a slow penetration rate, a high value for F_s can be chosen. Fitting F_s is reasonable in this model, as it facilitates the diffusion path length calculation, which currently cannot be found by a physical measurement (Riederer and Schreiber, 1995).

The aqueous pore density, η_{pore} , as described in **Table 2**, was high. It is close to densities found elsewhere of $2 \times 10^{15} \text{ m}^{-2}$ in *Citrus aurantium* cuticles (Schreiber and Schönherr, 2009, p. 85). A high value for pore density indicates penetration would be rapid, as the experimental data indicates.

The fitted parameter for the logistic decay evaporation term, χ , as described in **Table 2**, multiplies the evaporation in Equation (28) for CCA mode. Dash and Garimella (2013) found there was a need to include an extra constant in CCA mode with the Popov (2005) model, which they attribute to evaporative cooling at the droplet interface and a lower effective thermal conductivity of the substrate due to air gaps present on the surface.

Ion binding of AI onto the cuticle surface has been identified here as a key mechanism. Ionic penetration through plant cuticles can level out at less than 100% (Santier and Chamel, 1992; Schönherr, 2000, 2006; Kraemer et al., 2009). However, some of these studies have been plotted on a log plot, making analysis difficult. If penetration levels out and the rate of change of penetration is zero, penetration has ceased. Here we have identified that penetration levels out at less than 100% due to ion binding. One paper within the literature has shown ion binding exists (Yamada et al., 1964), another found differences between the adaxial and abaxial leaf surfaces (Horgan, 2017) and a third found penetration was different when the inner or outer cuticle surface was utilized (Santier and Chamel, 1992). However, the Yamada et al. (1964) paper is not well represented within the current literature. There is not yet a body of conclusive evidence to support it. The experimental techniques could perhaps be improved and expanded upon to include various plant species, ionic AIs, relative humidities and adjuvants. There could be additional mechanisms that interact with the ions, the ions could remobilize once bound, the ions could bind inside the cuticle aqueous pores and the mechanism could change with relative humidity or the addition of adjuvants.

We will explore the need to incorporate ion binding into the model numerically, investigating penetration of CaCl_2 with RSO 5 at $c_{\text{AI},0}^{\text{drop}} = 1 \text{ g/L}$, as shown in **Figure 11** and fitting parameters described in **Table S3**. We have fitted the data with 2 parameter sets. We have then removed the ion binding mechanism from the model by setting k to be zero. Without ion binding, as shown in **Figure 11**, it is not possible to fit the data and the root-mean-square errors, RMSE, are large (values closer to zero indicate better fits), as shown in **Table S3**. Therefore, ion binding is necessary to include within a penetration model.

Incorporating evaporation with the hygroscopic nature of ionic AIs into a mechanistic model, producing Equation (28), is a novel approach first published in this paper. This model could be useful for other circumstances such as sea salt mixed with spray formulations deposited onto foliage (Chen and Lee, 2001; Fernández et al., 2017;

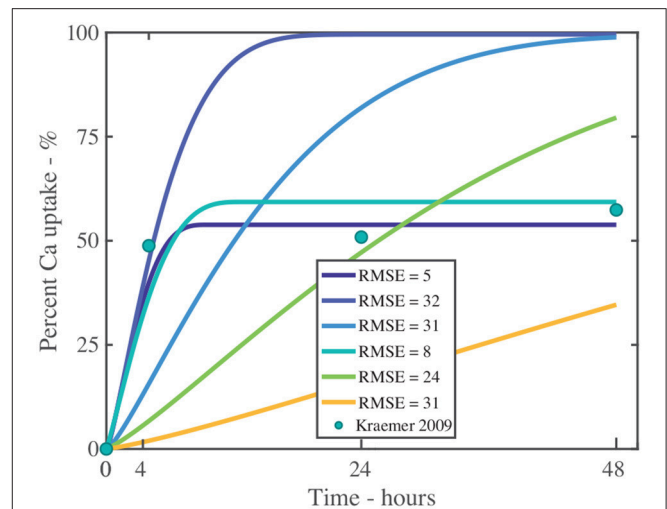


FIGURE 11 | Fitting experiment both with and without ion binding for a single applied initial concentration of 1 g/L or 5 μg and parameters described in **Table 2**. The experimental data is shown as green circles. The additional fitting parameters are described in **Table S3**. The root-mean-square error, RMSE, indicates the fit, where values closer to zero indicate improved fits.

Lovelock et al., 2017). The evaporation model can be thought to apply to any ionic hygroscopic solution on many types of substrates, not just plant cuticles.

The plant cuticle diffusion model can theoretically apply to the penetration of most ionic hydrophilic AIs, both with and without adjuvants. It can apply to isolated stomatous plant leaf or fruit species cuticle, where the aqueous pores are sufficiently large to allow AI to be transported through the cuticle via Fickian diffusion. It can be utilized to model changes in relative humidity, AI type and concentration, plant species variation, adjuvant type and POD of AI with adjuvant. Species where transport is extremely slow is theorized to be a mechanism other than Fickian diffusion. This requires further investigation before applying the model. The model cannot be applied to lipophilic compounds, ionic hydrophilic compounds such as Fe chelates (Schönherr et al., 2005; Schlegel et al., 2006) that dehydrate aqueous pores, uncharged hydrophilic compounds or whole leaf penetration. Simple adaptations could be made to this model to account for these cases, which will be the subject of future work.

Aqueous pores are known to change in size and swell with water adsorption (Luque et al., 1995; Kerstiens, 2006; Schönherr, 2006). Swelling of the aqueous pores also occurs while penetration takes place, is included within the model and is directly proportional to the concentration of water. The initial conditions for the experimental setup (Kraemer et al., 2009) are a water droplet on the cuticle surface, a water bath on the inner cuticle surface, rehydrated cuticle and aqueous pores that are fully swelled. As there is a high concentration of water initially that does not change significantly, pores do not swell to a large degree as the pore radius is directly proportional to the concentration of water. However, under other experimental setups, pore swelling may be significant. We surmise these could include an initially dry isolated cuticle or a cuticle that was initially in a low relative humidity, then was placed in a high humidity just prior to the experiment. We leave pore swelling here as it allows the model to be more adaptable, with the view to investigate such cases in future works.

5. CONCLUSION

A mechanistic model has been developed here to simulate diffusion of hydrophilic ionic active ingredients including adjuvants through plant cuticles. We have also included diffusion and adsorption of water within the cuticle. This model makes novel additions to a simple diffusion model by incorporating the important governing mechanisms of swelling of the aqueous pores, climatic conditions such as relative humidity that affect the evaporation of water in the applied droplet. We also include parameters that account for the differences in plant species, porosity and tortuosity of the aqueous pores, ion binding to the cuticle surface, a diffusivity function that changes in time through the cuticle and parameters capable of incorporating adjuvant addition with initial contact angle and point of deliquescence adjustment. Here we have developed novel additions to the Popov (2005) evaporation model, incorporating hygroscopic water absorption and point of deliquescence effects, which may be theoretically applied to any ionic hygroscopic solution on many types of substrates, not just plant cuticles. The model has been solved numerically, producing results that show reasonable agreement with the experimental data for both ionic AI and ionic AI including surfactant, by altering several parameters, but not changing the model itself. We have discussed mechanisms of ion binding, point of deliquescence and relative humidity that significantly limited penetration and were necessary to incorporate into a penetration model. Major factors influencing penetration were found with the sensitivity analysis to be plant species variations with cuticle structure including tortuosity, porosity, maximum pore radius, pore density, initial contact angle and cuticle thickness; ion binding, evaporation and hygroscopic growth parameters such as relative humidity. The sensitivity analysis indicated surfactants increase penetration by

changing the initial contact angle and changing the POD of a solution, which alters the water absorption of the solution. The results of the sensitivity analysis are in keeping with the well-established literature.

AUTHOR CONTRIBUTIONS

ET is responsible for article writing, model creation and adaptation, computational code creation, results, analysis, article editing and revision. TF is responsible for model creation and adaptation, results, analysis, article editing and revision. WF is responsible for motivating the project, the biological and agrochemical consultation, article editing and revision. All authors agree to be accountable for all aspects of the work in ensuring that questions related to the accuracy or integrity of any part of the work are appropriately investigated and resolved.

ACKNOWLEDGMENTS

We thank Steven Psaltis for his contribution to the development of the numerical scheme in the previous work (Tredenick et al., 2017). Computational resources and services used in this work were provided by the High Performance Computing and Research Support Group, Queensland University of Technology, Brisbane, Australia.

SUPPLEMENTARY MATERIAL

The Supplementary Material for this article can be found online at: <https://www.frontiersin.org/articles/10.3389/fpls.2018.01888/full#supplementary-material>

REFERENCES

- Absortech (2015). *Calcium Chloride: A Superior Choice Over Silica Gel*. Tokyo: Absortech Company.
- ASABE (2009). *American Society of Agricultural and Biological Engineers (ASABE) s572.1 Droplet Size Standard - Spray Nozzle Classification by Droplet Spectra*.
- Balneaves, J., Gaskin, R., and Zabkiewicz, J. (1993). The effect of varying rates of glyphosate and an organosilicone surfactant on the control of gorse. *Ann. Appl. Biol.* 122, 531–536. doi: 10.1111/j.1744-7348.1993.tb04055.x
- Bard, A. J., and Faulkner, L. R. (2001). *Electrochemical Methods: Fundamentals and Applications, 2nd Edn*. New York, NY: John Wiley.
- Baur, P. (1999). Surfactant effects on cuticular penetration of neutral polar compounds: dependence on humidity and temperature. *J. Agricult. Food Chem.* 47, 753–761. doi: 10.1021/jf980507h
- Beyer, M., Lau, S., and Knoche, M. (2005). Studies on water transport through the sweet cherry fruit surface: IX. Comparing permeability in water uptake and transpiration. *Planta* 220, 474–485. doi: 10.1007/s00425-004-1354-y
- Bouzenada, S., Kaabi, A., Frainkin, L., Salmon, T., and Léonard, A. (2016). Experimental comparative study on lithium chloride and calcium chloride desiccants. *Proc. Comput. Sci.* 83, 718–725. doi: 10.1016/j.procs.2016.04.159
- Buchholz, A. (2006). Characterization of the diffusion of non-electrolytes across plant cuticles: properties of the lipophilic pathway. *J. Exp. Bot.* 57, 2501–2513. doi: 10.1093/jxb/erl023
- Burkhardt, J., and Hunsche, M. (2013). Breath figures on leaf surfaces—formation and effects of microscopic leaf wetness. *Front. Plant Sci.* 4:422. doi: 10.3389/fpls.2013.00422
- Chamel, A., Pineri, M., and Escoubes, M. (1991). Quantitative determination of water sorption by plant cuticles. *Plant Cell Environ.* 14, 87–95. doi: 10.1111/j.1365-3040.1991.tb01374.x
- Chandra, S., di Marzo, M., Qiao, Y., and Tartarini, P. (1996). Effect of liquid-solid contact angle on droplet evaporation. *Fire Safety J.* 27, 141–158. doi: 10.1016/S0379-7112(96)00040-9
- Chen, Y., and Lee, W. G. (2001). The effect of surfactants on the deliquescence of sodium chloride. *J. Environ. Sci. Health A* 36, 229–242. doi: 10.1081/ESE-100102620
- Coret, J. M., and Chamel, A. R. (1993). Influence of some nonionic surfactants on water sorption by isolated tomato fruit cuticles in relation to cuticular penetration of glyphosate. *Pesticide Sci.* 38, 27–32. doi: 10.1002/ps.2780380105
- Dash, S., and Garimella, S. V. (2013). Droplet evaporation dynamics on a superhydrophobic surface with negligible hysteresis. *Langmuir* 29, 10785–10795. doi: 10.1021/la402784c
- Delele, M. A., Nuytens, D., Duga, A. T., Ambaw, A., Lebeau, F., Nicolai, B. M., et al. (2016). Predicting the dynamic impact behaviour of spray droplets on flat plant surfaces. *Soft Matter* 12, 7195–7211. doi: 10.1039/C6SM00933F
- Doganci, M. D., Sesli, B. U., and Erbil, H. Y. (2011). Diffusion-controlled evaporation of sodium dodecyl sulfate solution drops placed on a hydrophobic substrate. *J. Coll. Interface Sci.* 362, 524–531. doi: 10.1016/j.jcis.2011.06.060
- Dow Chemical Company (2003). *Calcium Chloride Handbook a Guide to Properties, Forms, Storage and Handling*. Michigan, MI: Dow Chemical Company.
- Erbil, H. Y. (2012). Evaporation of pure liquid sessile and spherical suspended drops: a review. *Adv. Coll. Interf. Sci.* 170, 67–86. doi: 10.1016/j.jcis.2011.12.006
- Erbil, H. Y., McHale, G., and Newton, M. I. (2002). Drop evaporation on solid surfaces: constant contact angle mode. *Langmuir* 18, 2636–2641. doi: 10.1021/la011470p
- Fedorov, V. V. (1972). *Theory of Optimal Experiments*. New York, NY: Elsevier.
- Fernández, V., Bahamonde, H. A., Javier Peguero-Pina, J., Gil-Pelegrín, E., Sancho-Knapik, D., Gil, L., et al. (2017). Physico-chemical properties of plant cuticles and their functional and ecological significance. *J. Exp. Bot.* 68, 5293–5306. doi: 10.1093/jxb/erx302

- Forster, W. A., Zabkiewicz, J. A., and Riederer, M. (2004). Mechanisms of cuticular uptake of xenobiotics into living plants: 1. Influence of xenobiotic dose on the uptake of three model compounds applied in the absence and presence of surfactants into *Chenopodium album*, *Hedera helix* and *Stephanotis floribunda* leaf. *Pest Manage. Sci.* 60, 1105–1113. doi: 10.1002/ps.918
- Forster, W. A., Zabkiewicz, J. A., and Riederer, M. (2006). Mechanisms of cuticular uptake of xenobiotics into living plants: evaluation of a logistic-kinetic penetration model. *J. Agricult. Food Chem.* 54, 3025–3032. doi: 10.1021/jf0528916
- Gaskin, R. E., Steele, K. D., and Forster, W. A. (2005). Characterising plant surfaces for spray adhesion and retention. *N. Z. Plant Protect.* 58, 179–183. Available online at: <https://www.cabdirect.org/cabdirect/abstract/20053189311>
- Giles, C. H., Smith, D., and Huitson, A. (1974). A general treatment and classification of the solute adsorption isotherm. I. Theoretical. *J. Coll. Interf. Sci.* 47, 755–765. doi: 10.1016/0021-9797(74)90252-5
- Grasselli, M., and Pelinovsky, D. (2008). *Numerical Mathematics*. Sudbury, MA: Jones & Bartlett Learning.
- Haefs, R., Schmitz-Eiberger, M., Mainx, H. G., Mittelstaedt, W., and Noga, G. (2002). Studies on a new group of biodegradable surfactants for glyphosate. *Pest Manage. Sci.* 58, 825–833. doi: 10.1002/ps.539
- Hazen, J. L. (2000). Adjuvants: terminology, classification, and chemistry. *Weed Technol.* 14, 773–784. doi: 10.1614/0890-037X(2000)014[0773:ATCAC]2.0.CO;2
- Holz, M., Heil, S. R., and Sacco, A. (2000). Temperature-dependent self-diffusion coefficients of water and six selected molecular liquids for calibration in accurate 1H NMR PFG measurements. *Phys. Chem. Chem. Phys.* 2, 4740–4742. doi: 10.1039/b005319h
- Horgan, D. (2017). The uptake of phosphorus acid sprays into kauri foliage. *N. Z. Plant Protect.* 70:326. doi: 10.30843/nzpp.2017.70.96
- Hsu, K. H. (1983). A diffusion model with a concentration-dependent diffusion coefficient for describing water movement in legumes during soaking. *J. Food Sci.* 48, 618–622. doi: 10.1111/j.1365-2621.1983.tb10803.x
- Hunsche, M., and Noga, G. (2012). Effects of relative humidity and substrate on the spatial association between glyphosate and ethoxylated seed oil adjuvants in the dried deposits of sessile droplets. *Pest Manage. Sci.* 68, 231–239. doi: 10.1002/ps.2250
- Isla, R., and Aragües, R. (2009). Response of alfalfa (*medicago sativa* L.) to diurnal and nocturnal saline sprinkler irrigations. i: total dry matter and hay quality. *Irrigat. Sci.* 27, 497–505. doi: 10.1007/s00271-009-0167-y
- Jeffree, C. E. (2008). “The fine structure of the plant cuticle,” in *Annual Plant Reviews, Biology of the Plant Cuticle*, Vol. 23. eds M. Riederer and C. Muller (Oxford, UK: John Wiley & Sons), 11–126. doi: 10.1002/9780470988718.ch2
- Karbulková, J., Schreiber, L., Macek, P., and Šantrůček, J. (2008). Differences between water permeability of stomatous and stomatous cuticular membranes: effects of air humidity in two species of contrasting drought-resistance strategy. *J. Exp. Bot.* 59, 3987–3995. doi: 10.1093/jxb/ern238
- Kerstiens, G. (2006). Water transport in plant cuticles: an update. *J. Exp. Bot.* 57, 2493–2499. doi: 10.1093/jxb/erl017
- Kerstiens, G. (2010). “Plant cuticle,” in *Encyclopedia of Life Sciences (ELS)*, Chichester: John Wiley & Sons, 1–3. doi: 10.1002/9780470015902.a0002088.pub2
- Knoche, M. (1994). Effect of droplet size and carrier volume on performance of foliage-applied herbicides. *Crop Protect.* 13, 163–178. doi: 10.1016/0261-2194(94)90075-2
- Koch, K., Bhushan, B., and Barthlott, W. (2008). Diversity of structure, morphology and wetting of plant surfaces. *Soft Matter* 4, 1943–1963. doi: 10.1039/b804854a
- Kolthoff, I. M., Sandell, E. B., Meehan, E., and Bruckenstein, S. (1969). *Quantitative Chemical Analysis*, Vol. 826. London: Macmillan.
- Kraemer, T., Hunsche, M., and Noga, G. (2009). Cuticular calcium penetration is directly related to the area covered by calcium within droplet spread area. *Sci. Horticult.* 120, 201–206. doi: 10.1016/j.scienta.2008.10.015
- Lagarias, J. C., Reeds, J. A., Wright, M. H., and Wright, P. E. (1998). Convergence properties of the nelder–mead simplex method in low dimensions. *Soc. Indust. Appl. Math. J. Optim.* 9, 112–147. doi: 10.1137/S1052623496303470
- Lide, D. R., (ed.). (2004). *CRC Handbook of Chemistry and Physics, 84th Edn.* Florida, FL: CRC Press.
- Liu, J., and Nie, Y. (2001). Fractal scaling of effective diffusion coefficient of solute in porous media. *J. Environ. Sci.* 13, 170–172.
- Loucks, R. G., Reed, R. M., Ruppel, S. C., and Hammes, U. (2012). Spectrum of pore types and networks in mudrocks and a descriptive classification for matrix-related mudrock pores. *AAPG Bull.* 96, 1071–1098. doi: 10.1306/08171111061
- Lovelock, C. E., Reef, R., and Ball, M. C. (2017). Isotopic signatures of stem water reveal differences in water sources accessed by mangrove tree species. *Hydrobiologia.* 803, 133–145. doi: 10.1007/s10750-017-3149-8
- Luque, P., Gavara, R., and Heredia, a. (1995). A study of the hydration process of isolated cuticular membranes. *New Phytol.* 129, 283–288. doi: 10.1111/j.1469-8137.1995.tb04298.x
- MATLAB (2017). *Version 9.3 (R2017b)*. Natick, MA: The MathWorks Inc.
- Mays, T. (2007). A new classification of pore sizes. *Stud. Surf. Sci. Catal.* 160, 57–62. doi: 10.1016/S0167-2991(07)80009-7
- McKenna, C., Gaskin, R., Horgan, D., Dobson, S., and Jia, Y. (2013). Efficacy of a postharvest spirotramat spray against armoured scale insects on kiwifruit vines. *N. Z. J. Crop Horticult. Sci.* 41, 105–116. doi: 10.1080/01140671.2013.784710
- Mercer, G. N. (2007). A simple diffusion model of the effect of droplet size and spread area on foliar uptake of hydrophilic compounds. *Pesticide Biochem. Physiol.* 88, 128–133. doi: 10.1016/j.pestbp.2006.10.004
- Middleton, L. J., and Sanderson, J. (1965). The uptake of inorganic ions by plant leaves. *J. Exp. Bot.* 16, 197–215. doi: 10.1093/jxb/16.2.197
- Nairn, J., Forster, W., and Leeuwen, R. (2013). Universal spray droplet adhesion model—accounting for hairy leaves. *Weed Res.* 53, 407–417. doi: 10.1111/wre.12039
- Oakes, C. S., Simonson, J. M., and Bodnar, R. J. (1995). Apparent molar volumes of aqueous calcium chloride to 250°C, 400 bars, and from molalities of 0.242 to 6.150. *J. Solut. Chem.* 24, 897–916. doi: 10.1007/BF00973444
- Oxy Chemical Company (2014). *Calcium Chloride Properties*. Dallas, TX: Occidental Chemical Corporation (OxyChem).
- Pecha, J., Fürst, T., Kolomazník, K., Friebrová, V., and Svoboda, P. (2012). Protein biostimulant foliar uptake modeling: the impact of climatic conditions. *Am. Inst. Chem. Eng. J.* 58, 2010–2019. doi: 10.1002/aic.12739
- Picknett, R., and Bexon, R. (1977). The evaporation of sessile or pendant drops in still air. *J. Coll. Interf. Sci.* 61, 336–350. doi: 10.1016/0021-9797(77)90396-4
- Popov, Y. O. (2005). Evaporative deposition patterns: spatial dimensions of the deposit. *Phys. Rev. E* 71:036313. doi: 10.1103/PhysRevE.71.036313
- Popp, C., Burghardt, M., Friedmann, A., and Riederer, M. (2005). Characterization of hydrophilic and lipophilic pathways of *Hedera helix* L. cuticular membranes: permeation of water and uncharged organic compounds. *J. Exp. Bot.* 56, 2797–2806. doi: 10.1093/jxb/eri272
- Prüm, B., Seidel, R., Bohn, H. F., and Speck, T. (2011). Plant surfaces with cuticular folds are slippery for beetles. *J. R. Soc. Interf.* 9, 127–135. doi: 10.1098/rsif.2011.0202
- Ramsey, R., Stephenson, G., and Hall, J. (2005). A review of the effects of humidity, humectants, and surfactant composition on the absorption and efficacy of highly water-soluble herbicides. *Pesticide Biochem. Physiol.* 82, 162–175. doi: 10.1016/j.pestbp.2005.02.005
- Riederer, M., and Muller, C. (2008). *Annual Plant Reviews, Biology of the Plant Cuticle*, Vol. 23. Oxford, UK: John Wiley & Sons.
- Riederer, M., and Schreiber, L. (1995). “Waxes: the transport barriers of plant cuticles,” in *Waxes: Chemistry, Molecular Biology and Functions*, Vol. 6, ed R. Hamilton (Dundee: The Oily Press), 131–156.
- Riederer, M., and Schreiber, L. (2001). Protecting against water loss: analysis of the barrier properties of plant cuticles. *J. Exp. Bot.* 52, 2023–2032. doi: 10.1093/jxb/52.363.2023
- Saltelli, A., Ratto, M., Andres, T., Campolongo, F., Cariboni, J., Gatelli, D., et al. (2008). *Global Sensitivity Analysis: The Primer*. Chichester: John Wiley & Sons.
- Santier, S., and Chamel, A. (1992). Penetration of glyphosate and diuron into and through isolated plant cuticles. *Weed Res.* 32, 337–347. doi: 10.1111/j.1365-3180.1992.tb01894.x
- Satchivi, N. M., Stoller, E. W., Wax, L. M., and Briskin, D. P. (2000). A nonlinear dynamic simulation model for xenobiotic transport and whole plant allocation following foliar application. I. Conceptual foundation for model development. *Pesticide Biochem. Physiol.* 68, 67–84. doi: 10.1006/pest.2000.2501

- Schlegel, T. K., Schönherr, J., and Schreiber, L. (2006). Rates of foliar penetration of chelated Fe (III): role of light, stomata, species, and leaf age. *J. Agricult. Food Chem.* 54, 6809–6813. doi: 10.1021/jf061149i
- Schönherr, J. (2000). Calcium chloride penetrates plant cuticles via aqueous pores. *Planta* 212, 112–118. doi: 10.1007/s004250000373
- Schönherr, J. (2001). Cuticular penetration of calcium salts: effects of humidity, anions, and adjuvants. *J. Plant Nutr. Soil Sci.* 164, 225–231. doi: 10.1002/1522-2624(200104)164:2<225::AID-JPLN225>3.0.CO;2-N
- Schönherr, J. (2002). A mechanistic analysis of penetration of glyphosate salts across stomatous cuticular membranes. *Pest Manage. Sci.* 58, 343–351. doi: 10.1002/ps.462
- Schönherr, J. (2006). Characterization of aqueous pores in plant cuticles and permeation of ionic solutes. *J. Exp. Bot.* 57, 2471–2491. doi: 10.1093/jxb/erj217
- Schönherr, J., Fernández, V., and Schreiber, L. (2005). Rates of cuticular penetration of chelated Fe-III: role of humidity, concentration, adjuvants, temperature, and type of chelate. *J. Agricult. Food Chem.* 53, 4484–4492. doi: 10.1021/jf050453t
- Schönherr, J., and Lubner, M. (2001). Cuticular penetration of potassium salts: effects of humidity, anions, and temperature. *Plant Soil* 236, 117–122. doi: 10.1023/A:1011976727078
- Schönherr, J., and Riederer, M. (1989). “Foliar penetration and accumulation of organic chemicals in plant cuticles,” in *Reviews of Environmental Contamination and Toxicology*, ed G. W. Ware, Vol. 108 (New York, NY: Springer), 1–70.
- Schönherr, J., and Schmidt, W. (1979). Water permeability of plant cuticles. Dependence of permeability coefficients of cuticular transpiration on vapour pressure saturation deficit. *Planta* 144, 391–400.
- Schönherr, J., and Schreiber, L. (2004). Size selectivity of aqueous pores in stomatous cuticular membranes isolated from populus canescens (aiton) sm. leaves. *Planta* 219, 405–411. doi: 10.1007/s00425-004-1239-0
- Schreiber, L. (2005). Polar paths of diffusion across plant cuticles: new evidence for an old hypothesis. *Ann. Bot.* 95, 1069–1073. doi: 10.1093/aob/mci122
- Schreiber, L., Elshatshat, S., Koch, K., Lin, J., and Santrucek, J. (2006). AgCl precipitates in isolated cuticular membranes reduce rates of cuticular transpiration. *Planta* 223, 283–290. doi: 10.1007/s00425-005-0084-0
- Schreiber, L., and Schönherr, J. (2009). *Water and Solute Permeability of Plant Cuticles: Measurement and Data Analysis*, Vol. 616. Heidelberg: Springer.
- Semenov, S., Trybala, A., Agogo, H., Kovalchuk, N., Ortega, F., Rubio, R. G., et al. (2013). Evaporation of droplets of surfactant solutions. *Langmuir* 29, 10028–10036. doi: 10.1021/la401578v
- Semenov, S., Trybala, A., Rubio, R. G., Kovalchuk, N., Starov, V., and Velarde, M. G. (2014). Simultaneous spreading and evaporation: recent developments. *Adv. Coll. Interf. Sci.* 206, 382–398. doi: 10.1016/j.cis.2013.08.006
- Shampine, L. F. (2002). Solving $0 = f(t, y(t), y'(t))$ in matlab. *J. Numer. Math.* 10, 291–310. doi: 10.1515/JNMA.2002.291
- Shaner, D. L., and Beckie, H. J. (2014). The future for weed control and technology. *Pest Manage. Sci.* 70, 1329–1339. doi: 10.1002/ps.3706
- Stauber, J. M., Wilson, S. K., Duffy, B. R., and Sefiane, K. (2015). On the lifetimes of evaporating droplets with related initial and receding contact angles. *Phys. Fluids* 27:122101. doi: 10.1063/1.4935232
- Tang, I. N., Tridico, a. C., and Fung, K. H. (1997). Thermodynamic and optical properties of sea salt aerosols. *J. Geophys. Res.* 102:23269. doi: 10.1029/97JD01806
- Trapp, S. (2004). Plant uptake and transport models for neutral and ionic chemicals. *Environ. Sci. Pollut. Res. Int.* 11, 33–39. doi: 10.1065/espr2003.08.169
- Tredenick, E. C., Farrell, T. W., Forster, W. A., and Psaltis, S. T. P. (2017). Nonlinear porous diffusion modeling of hydrophilic ionic agrochemicals in stomatous plant cuticle aqueous pores: a mechanistic approach. *Front. Plant Sci.* 8:746. doi: 10.3389/fpls.2017.00746
- Veraverbeke, E. A., Verboven, P., Van Oostveldt, P., and Nicolai, B. M. (2003). Prediction of moisture loss across the cuticle of apple (*malus sylvestris* subsp. *mitis* (wallr.)) during storage: part 1. Model development and determination of diffusion coefficients. *Postharvest Biol. Technol.* 30, 75–88. doi: 10.1016/S0925-5214(03)00083-8
- Viougeas, M., Rohr, R., and Chamel, A. (1995). Structural changes and permeability of ivy (*Hedera helix* L.) leaf cuticles in relation to leaf development and after selective chemical treatments. *New Phytol.* 130, 337–348. doi: 10.1111/j.1469-8137.1995.tb01828.x
- Weast, R. C., and Lide, D. R. (eds.). (1989). *CRC Handbook of Chemistry and Physics, 70th Edn.* Boca Raton, FL: CRC Press, Inc.
- Wolfe, P. (1959). The secant method for simultaneous nonlinear equations. *Commun. Assoc. Comput. Machinery* 2, 12–13. doi: 10.1145/368518.368542
- Xu, L., Zhu, H., Ozkan, H. E., Bagley, W. E., and Krause, C. R. (2011). Droplet evaporation and spread on waxy and hairy leaves associated with type and concentration of adjuvants. *Pest Manage. Sci.* 67, 842–851. doi: 10.1002/ps.2122
- Yamada, Y., Wittwer, S., and Bukovac, M. (1964). Penetration of ions through isolated cuticles. *Plant Physiol.* 39:28. doi: 10.1104/pp.39.1.28
- Yeats, T. H., Martin, L. B. B., Viart, H. M.-F., Isaacson, T., He, Y., Zhao, L., et al. (2012). The identification of cutin synthase: formation of the plant polyester cutin. *Nat. Chem. Biol.* 8, 609–611. doi: 10.1038/nchembio.960
- Yuan, J., and Sundén, B. (2014). On mechanisms and models of multi-component gas diffusion in porous structures of fuel cell electrodes. *Int. J. Heat Mass Transf.* 69, 358–374. doi: 10.1016/j.ijheatmasstransfer.2013.10.032
- Yuan-Hui, L., and Gregory, S. (1974). Diffusion of ions in sea water and in deep-sea sediments. *Geochim. Cosmochim. Acta* 38, 703–714. doi: 10.1016/0016-7037(74)90145-8
- Zabkiewicz, J. A. (2007). Spray formulation efficacy – holistic and futuristic perspectives. *Crop Protect.* 26, 312–319. doi: 10.1016/j.cropro.2005.08.019
- Zen, E. (1957). Partial molar volumes of some salts in aqueous solutions. *Geochim. Cosmochim. Acta* 12, 103–122. doi: 10.1016/0016-7037(57)90022-4
- Zhou, Z.-L., Cao, C., Cao, L.-D., Zheng, L., Xu, J., Li, F.-M., et al. (2017). Evaporation kinetics of surfactant solution droplets on rice (*oryza sativa*) leaves. *PLoS ONE* 12:e0176870. doi: 10.1371/journal.pone.0176870

Conflict of Interest Statement: The authors declare that the research was conducted in the absence of any commercial or financial relationships that could be construed as a potential conflict of interest.

Copyright © 2018 Tredenick, Farrell and Forster. This is an open-access article distributed under the terms of the Creative Commons Attribution License (CC BY). The use, distribution or reproduction in other forums is permitted, provided the original author(s) and the copyright owner(s) are credited and that the original publication in this journal is cited, in accordance with accepted academic practice. No use, distribution or reproduction is permitted which does not comply with these terms.